THESIS

# EVAPORATIVE MOISTURE SOURCES OF COLORADO'S FRONT RANGE: A CASE STUDY OF THE EXCEPTIONALLY WET MAY-JULY SEASON OF 2023

Submitted by

Katherine V. Humphreys

Department of Atmospheric Science

In partial fulfillment of the requirements

For the Degree of Master of Science

Colorado State University

Fort Collins, Colorado

Summer 2025

Master's Committee:

Advisor: Patrick W. Keys

Russ S. Schumacher
Frances V. Davenport

# ABSTRACT


## EVAPORATIVE MOISTURE SOURCES OF COLORADO'S FRONT RANGE: A CASE STUDY OF THE EXCEPTIONALLY WET MAY-JULY SEASON OF 2023

In 2023, some of Colorado's eastern plains experienced its wettest three-month period (May - July) out of 129 years of record (Colorado Climate Center, 2024). This extreme precipitation led to flash flooding, road washouts, and significant property damage among Colorado communities along the Front Range including Denver, Boulder, and Fort Collins. Although much is known about the seasonality of precipitation in Colorado, few studies have explored the evaporative origin of precipitation in the Front Range. To better anticipate and understand extreme precipitation events across the Front Range, we investigated the evaporative origin of 2023's extreme precipitation and how it compares to moisture sources during the previous 23 years. Specifically, this study uses the Water Accounting Model 2 Layers (WAM2layers) and hourly ERA5 reanalysis data to quantify the sources of precipitation in Colorado's Front Range during the early summer of 2023 and over the past 23 years (2000-2023). Our moisture source analysis reveals that for the Front Range region in May-July of 2023: (1) the three primary moisture sources were the Pacific Ocean, the western United States, and Colorado itself, contributing just over 66.2% of total precipitation; (2) while these sources are historically dominant, terrestrial contributions and local moisture recycling (i.e., precipitation that recently evaporated from within the Front Range) accounted for a signiPatrickficantly larger share

than in prior years; (3) moisture sources in May-July 2023 were a statistical outlier in terms of the magnitude of moisture contributed to the Front Range, forming a cluster of its own relative to the past 24 years; and (4) between the two most dominant modes of variability, 2023 aligns more with a basin-wide pulsing pattern rather than a north-south dipole pattern of moisture sources. This research provides new insights into the extreme rainfall in the summer of 2023 as well as the historical origins of warm-season precipitation in the Front Range.

TABLE OF CONTENTS

# CHAPTER 1: INTRODUCTION

In May through July of 2023, parts of Eastern Colorado experienced its wettest three-month period out of 129 years of record, as seen in Figure 1. Multiple heavy and convective rain events during these months caused some regions across Eastern Colorado to receive over 16 inches of rain, exceeding their average annual precipitation. Out of Colorado's 5.7 million residents, the Front Range urban corridor is home to an estimated 4.9 million people as per the U.S. Census Bureau's 2020 census. This record-breaking rainfall affected many residents along the Front Range in the form of urban flooding, property damage, and infrastructure damage such as road washouts and sinkholes.

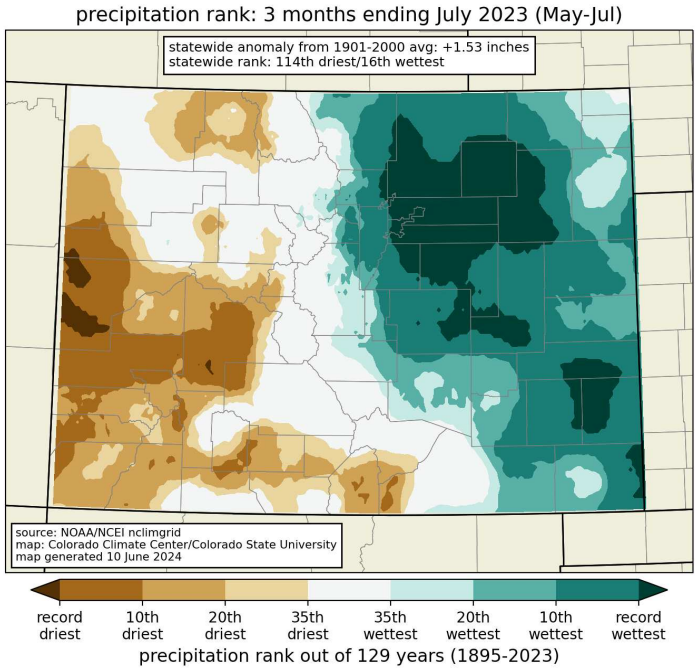


**Figure 1:** Ranking of precipitation from May-July 2023, compared to all 129 May-July periods in the PRISM precipitation dataset. The areas in darkest green had record-breaking wet conditions in 2023. Note, this Figure was created by the Colorado Climate Center (CCC) and was sourced from the CCC's Climate at a Glance webpage (Colorado Climate Center, 2024).

### 1.1 Moisture Source Research

One useful lens to study precipitation is through its source regions or evaluating where that moisture last evaporated from before falling as precipitation. Studying moisture sources provides insight into how water is exchanged between the surface and the atmosphere, overall, furthering our knowledge of the hydrologic cycle (Gimeno et al., 2020). This form of analysis is also specifically useful in identifying regions where precipitation patterns are vulnerable to land-use changes in upwind regions (Keys et al., 2016).

There is an extensive and growing body of research exploring extreme precipitation through the identification of its moisture sources and the associated pathways of water vapor transport. The specific moisture sources and mechanisms behind water vapor transport can vary considerably by location (Gimeno et al., 2020), so many researchers have opted to conduct regional analyses of precipitation at multiple timescales (i.e. multi month to sub weekly periods). Previous studies have explored the moisture sources of regions within Europe (e.g. Gustafson et al., 2010; Pinto et al. 2013; Rios-Entenza and Miguez-Macho, 2014; Ciric et al., 2018; Cloux et al., 2021), Asia (e.g. Zhao et al., 2016; Liu et al., 2021; Zhang et al., 2023; Liu et al., 2024; Zhang et al., 2024), Africa (e.g. Durmond et al., 2011; Rapolaki et al., 2021), South America (e.g. Arias et al., 2015; Marengo et al., 2013; Espinoza et al., 2014), and North America (e.g. Tan et al., 2018). There is also abundant research studying the moisture of precipitation in the United States, including regions that overlap Colorado's Front Range such as the Southwestern US (e.g. Jana et al., 2018; Erlingis et al 2019a; Erlingis et al., 2019b; Skinner et al., 2023), Midwestern US (e.g. Dirmeyer and Brubaker, 1999; Yang et al., 2023; Kim and Dominguez, 2023), and broadly across the country (e.g. Dirmeyer et al., 2009; Hu and Dominguez, 2015).

### 1.2 Colorado Precipitation & Moisture Sources

Since no major rivers flow into Colorado, the state receives almost all new water in the form of precipitation (Mckee et al., 2000). Thus, precipitation patterns throughout the year, especially within the wet season, govern key changes in drought conditions throughout the state. In general, the Front Range's wet season occurs in late spring to early summer months (Doesken, 2011). For example, Denver and the eastern foothills typically receive the most rainfall in May (Doesken et al., 2003). During the wet season, most of the precipitation in Eastern Colorado falls from convective thunderstorms forming over the mountains and moving eastward over the plains (Doesken, 2011).

In Colorado, the North American Monsoon (NAM) creates a circulation pattern favorable for transporting warm moist air from the Gulf of Mexico and the Gulf of California into Colorado's eastern plains (Mckee et al., 2000, Doesken et al., 2003). Although the North American Monsoon provides some predictability for moisture sources in the northern Front Range during July and August, this circulation typically does not strengthen until after peak rainfall in May and June. South of the Palmer Divide, however, peak precipitation occurs in July-August, coinciding with the onset of the Noth American Monsoon. While some studies have examined regional-scale source regions across multistate areas, such as the Upper Colorado River Basin (Kirk and Schmidlin, 2018) or the Southeastern U.S. (Skinner et al., 2023), others have focused on point-specific sites like Grand Junction in western Colorado and Eastville located just east of the Rocky Mountains (Jana et al., 2018). For the goals of our study, these efforts have added valuable insights, but they either cover too expansive a region or are too geographically limited to comprehensively represent the unique hydroclimatic characteristics of the Front Range.

While prior research has examined sources of moisture in the Southwestern US, limited attention has been given specifically to Colorado's Front Range, especially regarding the extremely wet conditions observed in 2023. This study aims to identify and quantify the evaporative sources of precipitation in Colorado's Front Range during its wet season (May - July), with an intentional focus on the exceptionally wet period from May through July 2023.

### 1.3 Study Goals

This study's goal is to better understand the extreme precipitation in 2023 by quantifying where it last evaporated from and putting those results into the context of the past 23 years. Exploring this region's historical sources of precipitation provides a baseline in which we can compare 2023 moisture sources to. These goals were designed to inform the emergency management team within the Colorado Water Conservation Board to whom this project is partially funded by. Although this paper focuses on Colorado's Front Range, these analyses were conducted for four other regions within Eastern Colorado and their results can be found in the appendix A.

The results reported here are organized into two main topics. First, we identify the moisture sources of Front Range precipitation across the three-month period and for individual months in May, June, and July of 2023. Second, we examine the average moisture sources of the Front Range from the past 23 years (2000-2022) and compare them to 2023.

# CHAPTER 2: METHODOLOGY

## 2.1 Water Vapor Tracking Methods

Precipitation in a given area can be thought of as the sum of two components: (1) moisture that evaporated remotely and advected into a region and (2) moisture that evaporated from within it (Burde and Zangvil, 2001). Moisture that evaporates from the land surface and returns as precipitation within the same region is a process called moisture recycling (Keys et al., 2012). To quantify the source regions of rainfall, it is essential to have a method for tracking water vapor as it moves through the atmosphere. Observational data related to moisture sources typically rely on measuring the stable isotopes of water to infer the origins of precipitation in the region. To address the goals of our study, these approaches are too spatially and temporally limited. Current methods of tracing water vapor through the atmosphere mostly rely on model-based tools that use numerical tracking methods. The types of numerical tracking methods can generally be defined by two characteristics: (1) whether the methods are online or offline and (2) whether they use a Lagrangian or Eulerian framework.

In online methods, water vapor tracking occurs concurrently as the weather or climate model progresses in time (e.g. Bosilovich and Schubert 2002; Knoche and Kunstmann, 2013; Rios-Entenza & Miguez-Macho, 2014). Offline methods are typically those that track moisture by using observational data, reanalysis data, and/or model output once it becomes available (e.g., Tuinenburg et al., 2012; Tuinenburg and Staal, 2020). Eulerian approaches track the budget of moisture that enters and exits a given column of atmosphere (e.g., van der Ent et al., 2010), while Lagrangian approaches track the pathway of moisture through time (e.g., Wei et al., 2013). This current work uses an Offline, Eulerian approach due to their inexpensive computational nature

compared to online, Lagrangian techniques. In the future, it would be interesting to explore and compare the results of this study through a Lagrangian model perspective.

**2.2 Model: WAM2layers**

To estimate the moisture for Colorado's Front Range, we used the WAM2layers Model (Water Accounting Model 2-Layers, v3.0.0-beta.5). This specific version of the WAM2layers used in this study can be downloaded from van der Ent et al. (2023), and more detailed information about version 3 can be found within Kalverla et al. (2024), currently a preprint at the time of writing this thesis. Previous versions of the WAM2layers are documented in van der Ent et al., (2010) and van der Ent et al., (2014). This section will first describe the model in general, how it was specifically used in this study, model assumptions, and close with other scholars who have used this model before.

The WAM2layers is an Offline, Eulerian model used to track water vapor forward and backward in time based on the conservation of atmospheric moisture or sometimes referred to as water balance (van der Ent et al., 2014). Instead of simulating atmospheric processes like a general circulation model, the WAM2layers acts as an accounting system that tracks the exchange of water vapor between grid cells using input meteorological data, most often a reanalysis dataset (Kalverla et al., 2024). Atmospheric moisture balance implies that the change in water vapor overtime must be equal to the horizontal and vertical fluxes in and out of the gridcell as well as the land-atmosphere moisture exchanges via evaporation and precipitation.

As the model's name suggests, the WAM2layers simplifies the atmosphere into two layers, an upper and a lower layer, to track the transport of water vapor. Within the model, this boundary typically occurs just above the planetary boundary layer with slightly more moisture contained in the lower layer on average. By default, the boundary between the upper and lower

layer of the atmosphere occurs in between levels 111 and 112 out of 137 total levels defined by the Integrated Forecasting System's (IFS) hybrid sigma-pressure vertical coordinate system, corresponding to about 812 hPa for a standard atmospheric surface pressure of 1013.25 hPa (Kalverla et al., 2024). Model resolution is dependent on the input data used which is described in the following section, section 2.3.

In this study, we only employed the backward tracking mode of the WAM2layers, or commonly called backtracking, to identify where Front Range precipitation last evaporated from. This backtracking process begins with global hourly meteorological data and a defined region of interest and then traces the precipitation backwards in time to where it most recently evaporated from. This process is then repeated over the indicated period. Output from backtracking consists of daily tracked evaporation data on a latitude longitude grid according to the resolution of the input meteorological data. Tracked evaporation is defined as the component of a given grid cell's total evaporation that will later fall as precipitation in the given region of interest (i.e. Colorado's Front Range defined in section 2.4).

For this research, we backtracked Front Range precipitation from 19 December 2023 to 1 January 2000. However, in our analysis, we do not include data from December, November, October, nor September of 2023 to allow over three months of spin-up time for the model. Since water vapor is estimated to have a short lifetime of around nine days on average (van der Ent et al., 2014; van der Ent and Tuinenburg, 2017), three months is ample time required for the WAM2layers to reach a stable state. Based on a sensitivity analysis, we also decided to run the WAM2layers with a limited domain of only the Northern Hemisphere from 80°N to 0°N/S to reduce the amount of core hours needed to run the model and store output. Reducing the domain to exclude the Southern Hemisphere did not dramatically affect the results of this study but did,

however, dramatically reduce the computational time of the model (Figure A.2.1 in the appendix). We also limited the domain to below 80°N latitude because, at high latitudes, the model's method for moving moisture between grid cells can lead to unrealistic distribution of water vapor, a known issue related to numerical diffusion (Kalverla et al., 2024).

**2.3 Data: ERA5 Reanalysis**

The WAM2layers relies on meteorological variables from the 0.25-degree latitude-longitude ERA5 Reanalysis dataset (Hersbach et al., 2020). For this project, we use variables measured hourly that include specific humidity, zonal and meridional wind speed, surface pressure, evaporation, and precipitation. In addition to the meteorological variables from ERA5, we also used ECMWF's land-sea mask to quantify the evaporative contributions of terrestrial versus aquatic regions. This land-sea mask assigns each cell a value ranging from 0 to 1 representing the cell's land to water ratio based on land surface calculations last updated in December of 2019. ERA5 is the most current version of the European Centre for Medium-Range Weather Forecasts' global climate reanalysis data product and performs well against precipitation observations in North America (Crossett et al., 2020; Beck et al., 2019; Tarek et al., 2020). Since the Front Range region sits just east of the Rocky Mountains, local details of precipitation are unable to be well represented.

### 2.4 Study Region: Colorado's Front Range

There are many geographical definitions of the Front Range, but we decided to use the Front Range region (FTR) of the alternate climate divisions developed for Colorado by Schumacher et al. (2024). That region was adapted to a quarter degree by quarter degree grid as depicted in Figure 2, and contains major cities such as Denver, Fort Collins, and Boulder. To be clear, these alternate climate divisions are not NOAA's (National Oceanic and Atmospheric Administration) official Climate Divisions that characterize Colorado regions by river basin. Instead, these alternate climate divisions characterize regions in Colorado by climate variability (Schumacher et al., 2024). For our specific purposes, we focus on the Front Range region of Colorado's Alternate Climate Divisions due to this region receiving extreme precipitation in May-July of 2023 and it is the most populous region among all 11 alternate climate divisions.

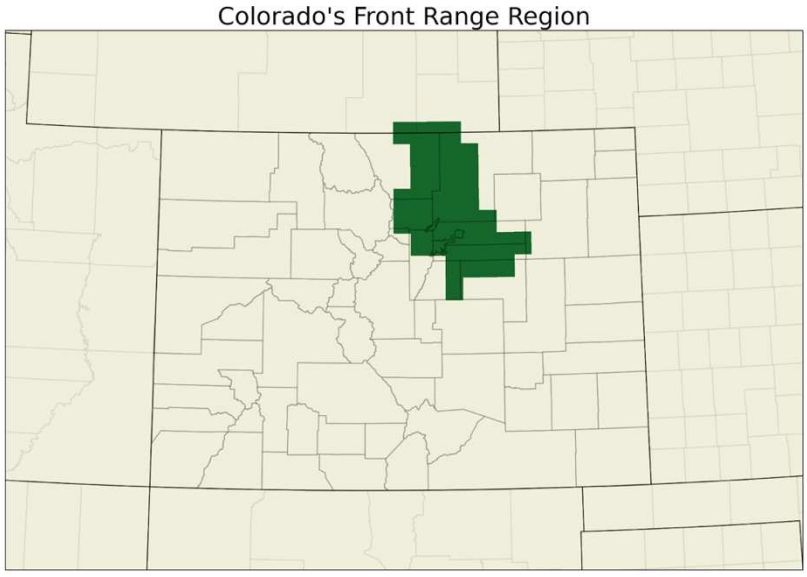


**Figure 2**: Map of Colorado depicting the Front Range region in green. Dark gray lines represent state boundaries, and the lighter gray lines represent county boundaries.

To note, this analysis was also conducted for the other four alternate climate divisions in Eastern Colorado (the Eastern Plains region, High Mountain Valley region, Pikes Peak region, and the Arkansas Basin region that also experienced an extremely wet May-July season in 2023. Results for these regions can be found in appendix A.

**2.5 K-Means Clustering Analysis**

To identify how moisture sources in 2023 compared to individual years instead of a climatological average, we applied a k-means clustering analysis to tracked-evaporation anomalies accumulated across May-July (MJJ) from 2000 to 2023. This method is an unsupervised machine learning algorithm chosen for its ease of physical interpretation and minimal required user inputs, reducing the interference from researcher specific bias. The goal of k-means clustering is to minimize the distance between each sample and the centroid of its assigned cluster and maximize the distance between the sample and centroids of different clusters (Loyd, 1982). For the purposes of this study, this method will group all twenty-four years (2000-2023) such that years with the most similar moisture source anomaly patterns will be sorted into the same group and that each cluster will be as distinct from each other as possible. This allows us to understand which individual MJJs are most similar to 2023, further putting this extreme year into context.

To do so, we used Scikit-Learn's k-means clustering algorithm as described in Pedregosa et al. (2012). As for every k-means analysis, we must decide and specify "k", i.e. the number of clusters to create. To select the optimal number of clusters for our data, we decided to use clustering metrics in combination with our personal knowledge of moisture sources to access the optimal number of clusters and avoid over-fitting. Since there are only twenty-four MJJ periods between 2000 and 2023, we decided to limit the maximum number of clusters to ten to avoid

over-fitting. Using more than ten clusters would decrease the interpretability of the results and inhibit our ability to contextualize moisture sources in MJJ of 2023. The further selection of our k value relies on a clustering metric, the elbow method. Results of the elbow method are described in section 3.3.

### 2.6 Empirical Orthogonal Function (EOF) Analysis

Empirical orthogonal function (EOF) analyses, sometimes referred to as principal component analysis (PCA), is a popular and robust method among the climate research community to study spatial patterns of the major modes of variability for a given variable. In moisture sources research, they have been applied to identify the spatial patterns of major modes of moisture source variability for a specific study region (e.g. Keys et al., 2014; Hu and Dominguez, 2015). In this study, we preprocessed tracked evaporation data by removing the grid cell mean with respect to time, leaving anomalous MJJ track evaporation anomalies to analyze. We then computed an EOF analysis on anomalous tracked evaporation accumulated over May, June, and July (MJJ) of a given year during 2000 to 2023. Our goal was to analyze how the moisture sources across MJJ of 2023 relate spatially to the major patterns of moisture source variability of Front Range precipitation. The first EOF is considered the eigenvector with the greatest associated eigenvalue that represents the spatial pattern that explains the most variance in Front Range moisture sources. In this study, we will focus on the two leading EOFs to better understand the Front Range's moisture source inter-annual variability and how moisture sources in 2023 compare. Due to memory constraints, we reduced the size of the data by only including data within the contiguous US and some of the surrounding oceans (67.0° W to 134.0° W longitude and 23.0° N to 49° N latitude). Our results are constrained to the portion of Front Range moisture sources within these bounds.

# CHAPTER 3: RESULTS

## 3.1 Moisture Sources of May, June, and July 2023 Precipitation

Here we discuss the moisture sources of Front Range precipitation in the months of May, June, and July of 2023 spatially (figure 3.a), by absolute regional contribution (3.b and 3.c.), and relative regional contributions (3.d and 3.e). Bar chart colors indicate the different evaporative source regions: terrestrial sources are shown in brown and yellow hues, with yellow representing moisture originating from within Colorado. Aquatic sources are depicted in teal and blue, representing contributions from the Atlantic and Pacific Ocean basins, respectively. The bar chart is stacked in such a way that contributions from aquatic source regions are stacked at the bottom, followed by terrestrial sources on the top for easy differentiation. In Figures 3.b and 3.c, the height of the bar charts represents the accumulated monthly volume of evaporation that will fall as precipitation in the Front Range region. Bar height in Figures 3.d and 3.e are all 100% to represent the proportion of regional contribution during the specified time.

To note, at the monthly and annual time scale, total (spatially summed) tracked evaporation can be considered equivalent to accumulated precipitation (van der Ent and Tuinenburg, 2017; Gimeno et al., 2021). Moving forward, total annual or monthly tracked evaporation can also be considered as annual or monthly total precipitation, subject to the limitations of ERA5 as outlined above. This section is organized as follows, first detailing the amount and composition of rainfall accumulation cumulatively across these three months and then individually thereafter.

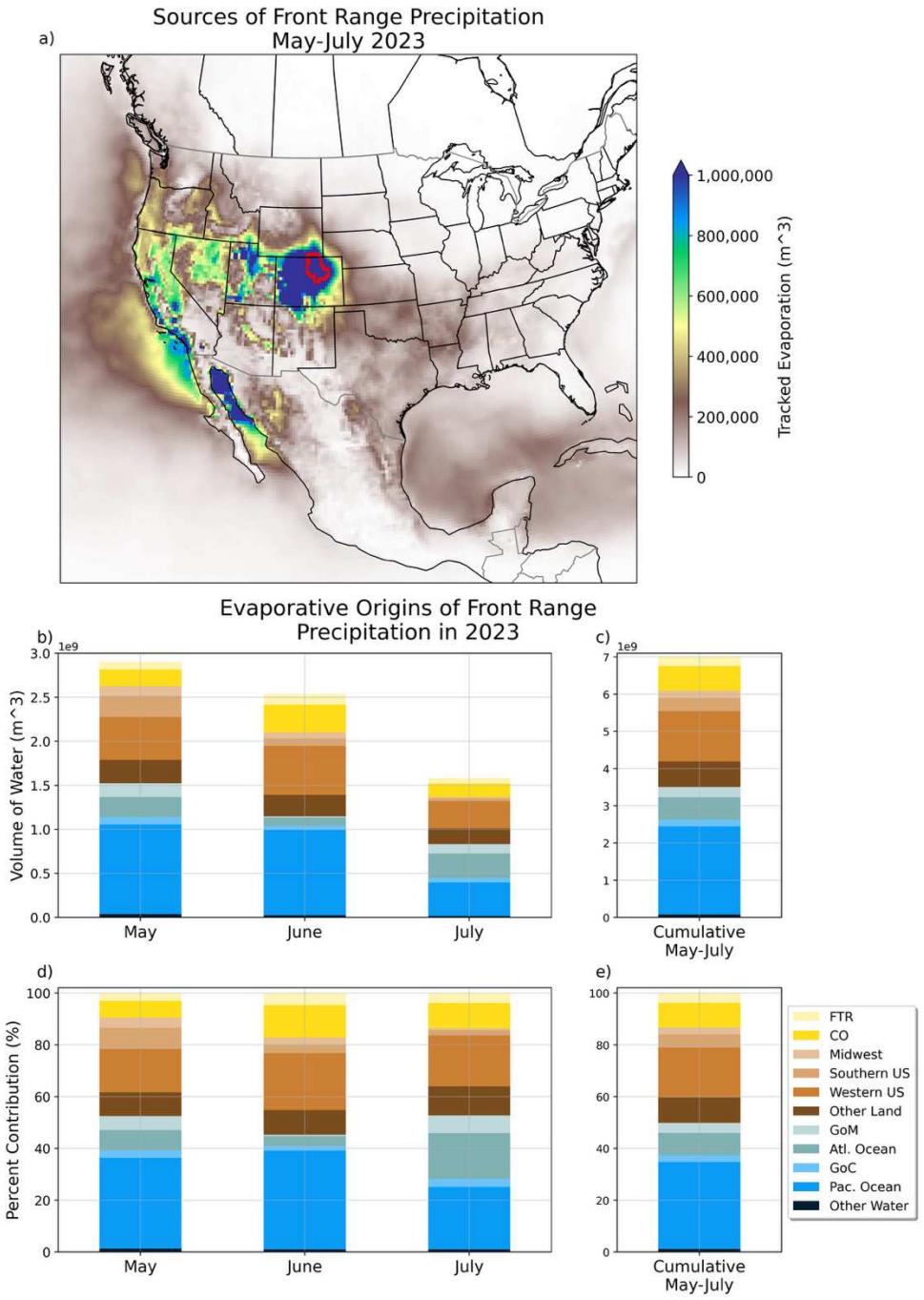


**Figure 3:** a), b), c), d), e) Spatial and monthly variation in moisture sources of Font Range (FTR) precipitation in May, June, and July of 2023. a) Map of evaporative sources of FTR precipitation accumulating from May through July of 2023. b) Monthly regional contribution to the FTR in volume of water vapor ($m^3$). c) Cumulative regional evaporative contribution across May, June and July of 2023 to FTR precipitation in volume of water vapor ($m^3$). d) Monthly regional evaporative contribution as a percent of total monthly evaporative contribution. e) Cumulative regional contribution as a percent of total monthly evaporative contribution. A map defining each of these regions is provided in the supplementary.

According to ERA 5 reanalysis data, the Front Range received just over 1.8 trillion gallons of water cumulatively in the late spring and early summer of 2023, equivalent to 13.3 inches of water covering the entire Front Range. Based on a 23-year average, this region typically accumulates 7.5 inches of precipitation across May, June, and July (MJJ). This almost doubling in MJJ precipitation aligns well with observations taken from this period and confirms the extreme nature of rainfall during this period.

Precipitation across May, June, and July of 2023 broadly originated from both terrestrial and aquatic areas spanning from the Northwest to the Southeast of the Front Range (FTR) with grid cells in Colorado, the Gulf of California, and Utah making up some of the greatest individual cell-based contributions (figure 3.a). In May through July of 2023, evaporation from terrestrial sources made up 50.1% of accumulated precipitation in the Front Range, whereas aquatic sources made up 49.9% (figure 3.e). Looking at regional contributions, the Pacific Ocean, Western US, and Colorado (including FTR) are the largest contributing regions by volume across the three-month period. These regions made up 33.7%, 19.3%, and 13.2% respectively of precipitation in the Front Range, or 66.2% of the precipitation combined in this three-month period (figure 3.e). Moisture recycling from within the FTR itself made up 3.8% of total precipitation during these three months or 269.6 million cubic meters of rainfall in absolute terms. The following text will discuss results from each month individually.

May 2023 is characterized as the wettest month of this MJJ period with multiple heavy, convective rainfall events producing just under 3 million cubic meters of water in total, equivalent to just over 5.5 inches of water covering the entire Front Range (Figure 3.b). Compared to the last 23 years, May 2023 received 167.9% of average May rainfall. Out of eleven regions, the three most contributing regions by volume were the Pacific Ocean, Western US, and Colorado (including the FTR) listed from greatest to least contribution. These regions made up 35.0%, 16.7%, and 9.5% respectively of Front Range precipitation, or 61.2% of precipitation combined (figure 3.d). From moisture evaporated from within the FTR, moisture recycling made up 3.0% (figure 3.d) of total monthly precipitation or, in absolute terms, 88.2 million cubic meters (figure 3.b) of water. Interestingly, regions such as the Southern US and the Gulf of Mexico may not be the largest contributors to May precipitation (figure 3.b), but in comparison to the last 23 years (figure 4.b), these regions contributed up to 5 times more water than they typically do this time of year.

June 2023 notably received the most anomalous amount of precipitation received in a single month that year, despite being the second wettest month. In total, the Front Range accumulated just over 4.8 inches of rain, 2.7 inches more than average June rainfall. This is 225.4% of average July rainfall throughout the past 23 years. In other words, June 2023 received over twice its usual amount of precipitation. The three most contributing moisture sources by volume were the Pacific Ocean, Western US, and Colorado (including the FTR), listed from greatest to least contribution. These regions made up 38.1%, 22.0%, and 17.3% respectively of Front Range precipitation, or 77.4% of precipitation combined (figure 3.d). Compared to May and July of 2023, the Atlantic Ocean and the Gulf of Mexico was less important to this anomalous precipitation in June (figure 3.b). In terms of moisture recycling, evaporation from

the FTR comprised 4.7% of total rainfall or 119.4 million cubic meters of water evaporated in the FTR returned as rainfall in the region during June (figure 3.b and 3.d).

July 2023 is designated by moderately above average precipitation and likely monsoonal influence. Total rainfall in July 2023 was equivalent to a depth of 3.0 inches of water, amounting to receiving 142.9% of average July precipitation over the last twenty-three Julys. In 2023, this month's three most contributing moisture sources to precipitation by volume were the Pacific Ocean, Western US, and Atlantic Ocean listed from greatest to least contribution. These regions made up 24.1%, 19.6%, and 17.6% of the total monthly precipitation respectively, or 61.3% of precipitation collectively (figure 3.d). The Atlantic Ocean is among the greater moisture sources in July, likely due to the onset of the North American Monsoon, known for being active throughout the late summer. This synoptic circulation pattern favors the advection of moisture from the Atlantic Ocean, Gulf of Mexico, and the Gulf of California into the region.

**3.2 Comparing 2023 to 23-Year Average**

The previous section established the moisture sources of extreme rainfall in May, June, and July of 2023 in the Front Range region; this section aims to compare how these results relate to the average of moisture sources from 2000-2022 (Figure 4.a-e). Since the moisture sources from the past twenty-three years are presented as an average instead of a single year (like figure 3.a-e), we defined average regional contribution as follows. First, we start by summing up the daily tracked evaporation in each time period (MJJ, month, etc.). Secondly, we take the summed tracked evaporation at each grid cell and take its mean through time, producing a map of average grid cell tracked evaporation in the given time period (Figure 4.a). To calculate the average regional tracked evaporation contribution, I then multiply the map in Figure 4.a by a binary mask of each region with 1 representing a grid cell inside the region and 0 indicating outside of the

source region. To be clear, the average regional contribution is not the simple average of regional contribution over time. We calculated the regional contributions such that their relative contributions all add up to 100%.

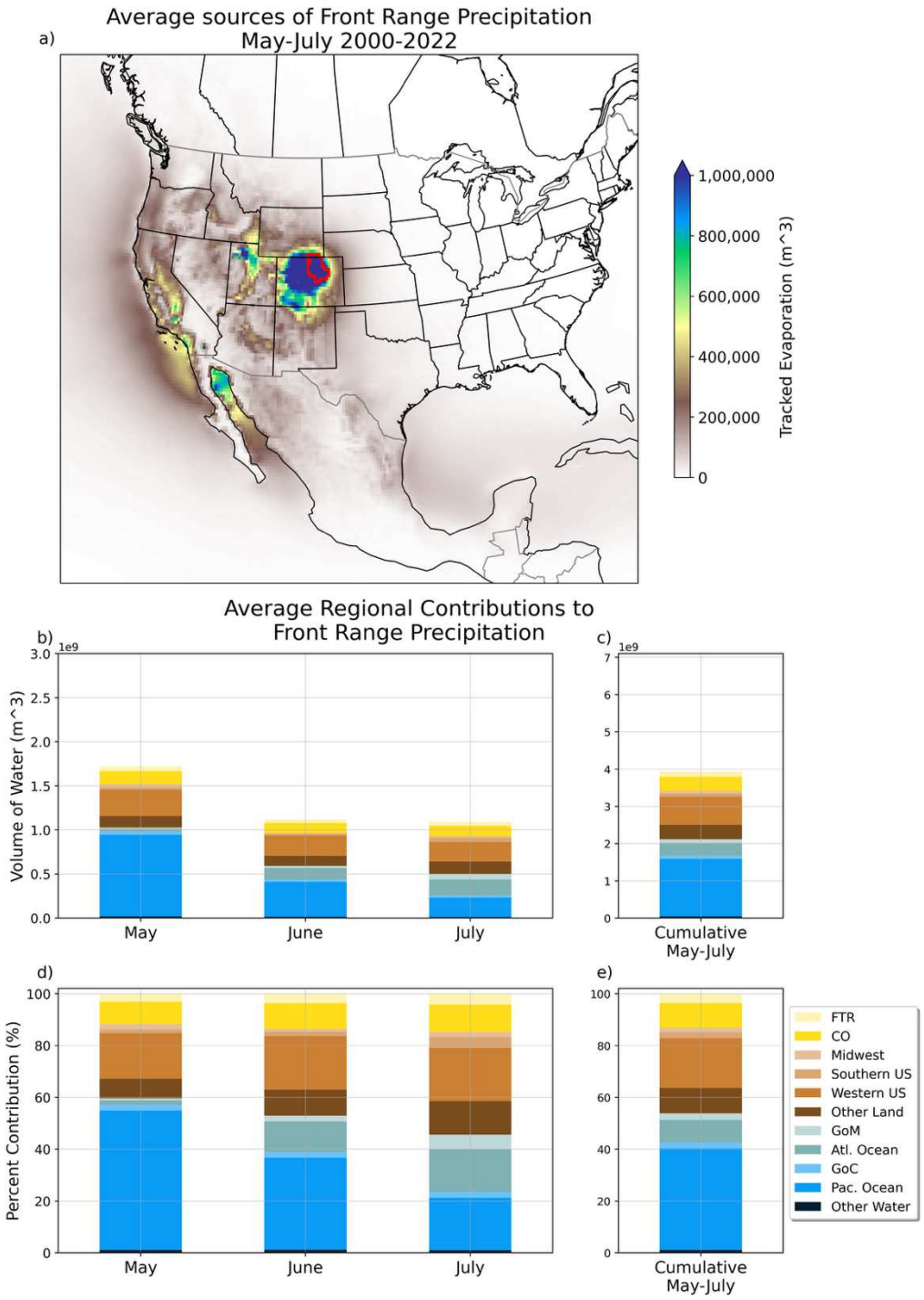


**Figure 4:** (a), (b), (c) Spatial and monthly variation of Front Range (FTR) moisture sources averaged from 2000-2022. (a) Map of average tracked evaporation accumulating from May through July. (b) Average monthly regional contributions to the FTR in volume of water vapor ($m^3$). (c) Average cumulative regional contribution across May, June and July to FTR precipitation in volume of water vapor ($m^3$). A map defining each of these regions is provided in the supplementary material.

Over the last 23 years, the Front Range (FTR) region typically accumulates 7.5 inches of precipitation across May, June, and July (MJJ). On average, rainfall during these three months mostly originated from aquatic and terrestrial areas directly to the west and southwest of the FTR. Comparatively, the moisture sources of MJJ rainfall in 2023 (Figure 3.a) originated from a much broader range of regions than the average moisture sources from the past 23-years (Figure 4.a). For example, grid cells in regions like the Midwest, Southeastern US, and the Gulf of Mexico have historically contributed less than 100,000 $m^3$ of water (Figure 4.a) in MJJ, whereas in 2023, many of these grid cells contributed >200,000 $m^3$ (figure 3.a) of water during the same timeframe shaded in brown hues.

In May through July, evaporation from terrestrial regions have on average made up 46.2% of precipitation in the Front Range, whereas aquatic sources made up 53.8% of precipitation. In 2023, terrestrial moisture sources (represented by brown and yellow hues of Figure 4.c and 3.c) increased their contribution from an average of 2.1 billion cubic meters of water (Figure 4.c) to 3.5 billion cubic meters (figure 3.c) in May through July. Not only did terrestrial surfaces contribute water vapor to the FTR, but these regions also made up a greater proportion of total MJJ rainfall increasing from 46.2% on average to 50.1% in 2023.

Over the past 23 years, the three regions that contributed the most to FTR rainfall across MJJ on average are the Pacific Ocean, the Western US, and Colorado itself (including FTR) (Figure 4.c). Respectively, these regions made up 39.3%, 19.2%, and 13.1% of MJJ rainfall on average, or 71.6% cumulatively. These three regions were also the largest moisture sources in 2023 (figure 3.c). According to these estimates, this means that the usual most important regions (in terms of volume of water contributed to FTR precipitation) remained the most important in 2023, but these major source regions shared a smaller proportion of the total MJJ precipitation.

Differing by 5.4% compared to the average share of FTR rainfall (71.6%). Although the largest moisture sources still did contribute more volume of water in 2023 (Figures 3.c and 4.c) than on average, smaller moisture sources (in terms of volume of water contributed) must have contributed twice or three times as much to account for the observed decrease in the largest moisture sources share of FTR precipitation in 2023.

Less dominant regions, such as the Midwest, Southeastern US, and Gulf of Mexico, contributed to extreme precipitation in May, June, and July (MJJ) of 2023 by contributing up to 4 times the amount of water they typically contribute on average. Typically, these regions contribute 73.2, 88.2, 99.5 million cubic meters of water to FTR precipitation respectively (Figure 4.c), whereas they contributed 193.1, 353.6, and 274.7 million cubic meters in May through July of 2023 (Figure 3.c). Although these regions still only account for 2.7%, 5.0%, and 3.9% of FTR precipitation in 2023 respectively, the Midwestern US contributed 2.6x, the Southern US contributed 4.0x, and the Gulf of Mexico contributed 2.8x the volume of water than they have on average. Not only did these regions contribute much larger amounts of moisture, they also made-up greater proportions of FTR precipitation in 2023 as alluded to in the paragraph above.

Ultimately, this suggests that 2023's extreme precipitation mostly originated from its most typical source regions, rather than being driven by an anomalous influx of moisture from an atypical location. However, smaller regions may have enhanced the anomalous amount of moisture reaching the FTR by contributing up to 4x their usual amount of moisture.

### 3.3 Clustering of Interannual Evaporation Patterns

To contextualize the moisture sources in 2023 with individual years, we applied a k-means clustering analysis to MJJ tracked evaporation anomalies from 2000-2023. The elbow method is one of the most popular methods used to determine optimal k values. This method is often criticized for its subjectivity when the 'crook' of the elbow is not well defined. However, as seen in figure 5, we believe the crook of the elbow is clear and well defined. This method identifies the optimal number of clusters by calculating the within-cluster sum of the squared errors (WCSS) between all samples and their identified centroid. The optimal cluster number is apparent when adding more clusters does not significantly reduce the WCSS significantly (Syakur et al., 2018). As shown in figure 5, after k values of three or four, WCSS decreases minimally. As such, we decided to use three clusters in efforts to strike a balance between model simplicity and capturing meaningful structure in the data.

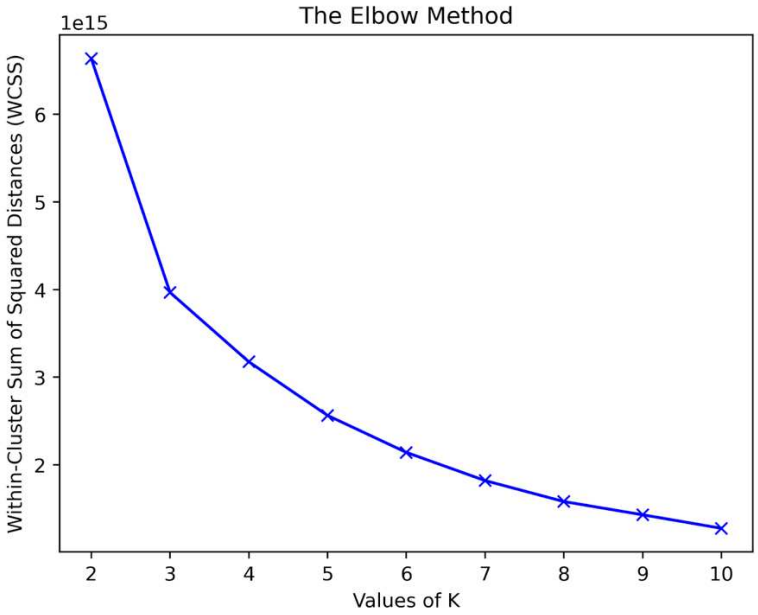


**Figure 5:** The elbow method with within-cluster sum of the squared error on the y axis and k, the number of specified clusters, plotted on the x axis. Before WCSS was calculated, the centroid clusters were calculated iteratively 100 times.

K-means clustering is an unsupervised machine learning technique and we use it to group the twenty-four MJJs into three distinct categories with similar spatial patterns. The results shown below are after 10,000 iterations to ensure a stable convergence of the clusters. Figure 6.a-c describes the average MJJ tracked-evaporation anomaly pattern for each cluster. Figure 6.d is a time series of the spatially summed tracked evaporation for a given MJJ. At the 3-month timeframe, total tracked evaporation is also equivalent to total precipitation (van der Ent and Tuinenburg, 2017; Gimeno et al., 2021). Each MJJ is then colored by what cluster they were assigned to.

Clusters one and two represent years with generally increased or decreased moisture contributions from Colorado, along with modest shifts in contributions from the Pacific Ocean, Gulf of California, and Western US (Figures 6.a and 6.b). From analysis in section 3.2, these regions closely coincide with major moisture sources of Front Range precipitation. Essentially, these two clusters distinguish between years with a surplus (cluster one) or deficit (cluster two) of moisture from largely local source regions. Figure 6.d describes the years assigned to each cluster as well as the total Front Range precipitation associated with that given season. This graph hints that anomalous moisture especially from local sources within Colorado may coincide with drier or wetter wet seasons in the Front Range. Though this pattern is interesting, it serves mainly as context for interpreting the more unusual case of 2023, and further investigation sits outside of the scope of this project.

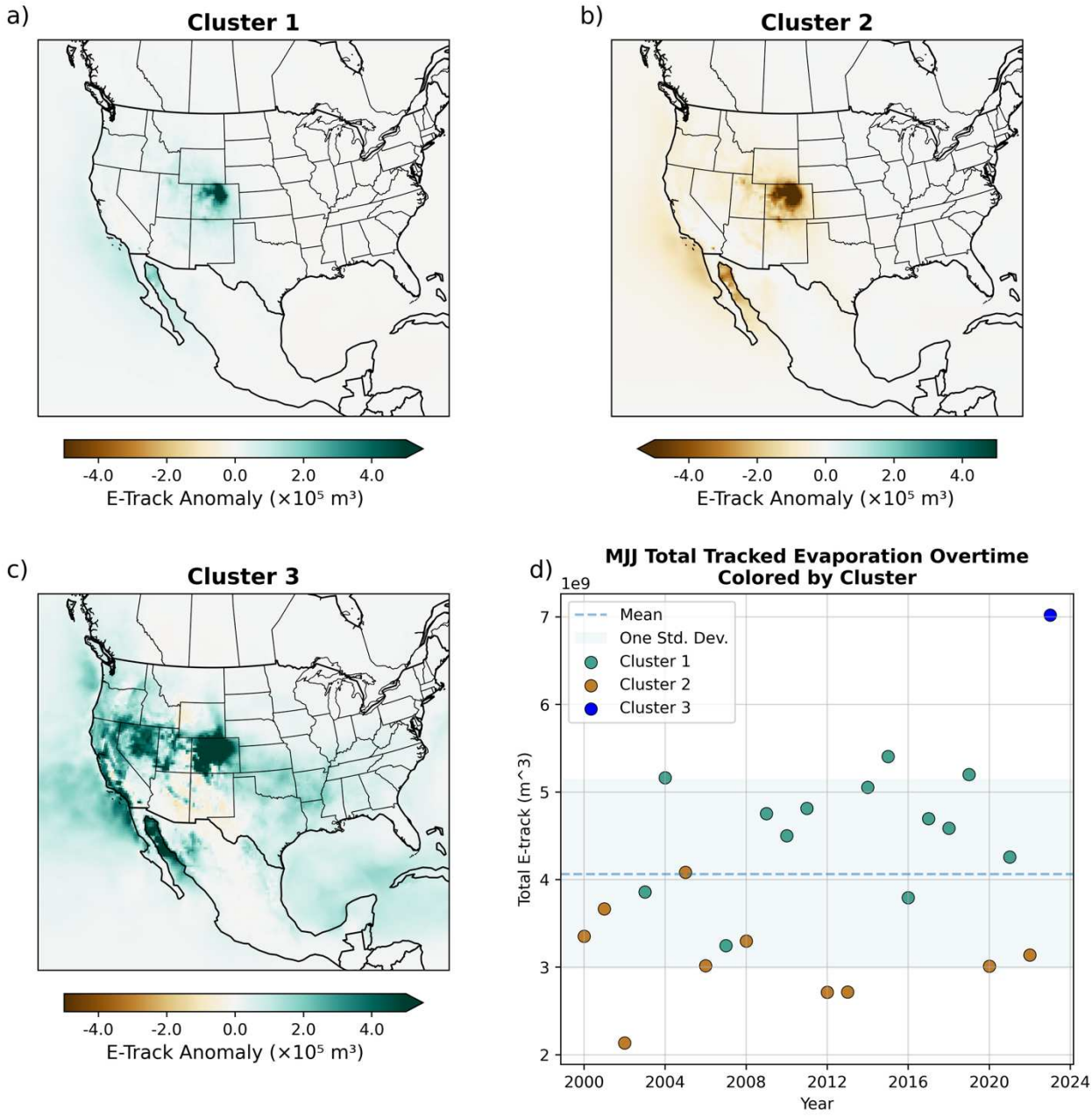


**Figure 6:** Spatiotemporal patterns of MJJ evaporation anomalies from k-means Clustering. (a), (b), (c) Cluster average MJJ moisture contribution. (d) MJJ total precipitation (spatially summed e-track) overtime colored by the assigned cluster.

MJJ of 2023 was the only year assigned to cluster three (Figure 6.d), making it an outlier in this 24-year record. As a result, the centroid in Figure 6.c reflects only 2023's tracked evaporation anomalies and is not a composite of multiple years. This separation from clusters one and two is interesting. Although 2023 shared the same dominant moisture sources (e.g. Colorado and the Pacific Ocean), the magnitude of contributions from those regions was dramatically higher than in any previous year. This extreme anomaly likely drove the clustering algorithm to isolate 2023 into its own group.

The distinctiveness of 2023 highlights how abnormally intense the moisture inflow was, despite the familiar major source regions. It suggests that while the spatial pattern of source region remains consistent with climatological norms found in previous sections, the volume of these contributions varied enough to distinguish 2023 entirely. This raises compelling questions about the cause of such intense moisture transport. Future research could examine the dynamical drivers behind moisture transport in the early summer of 2023. Although such interpretation is beyond the scope of this project, the isolation of 2023 underscores the value of moisture source tracking in identifying and contextualizing the nature of extreme hydroclimatic events.

### 3.4 Dominant Variability Patterns

In this last section of analysis, we identify the dominant variability patterns of MJJ season moisture sources using an empirical orthogonal function (EOF) analysis. Figure 7 illustrates the percent of variance explained (PVE) by a given eigenvector sorted from most to least variance explained. This value is determined by dividing the eigenvalue of a given eigenvector by the sum of all eigenvalues and multiplying by one hundred.

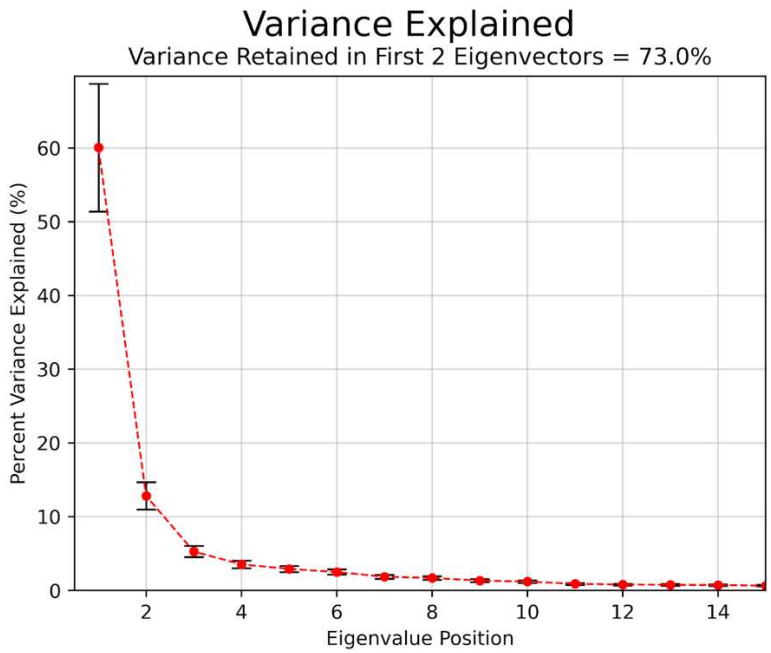


**Figure 7**: Percent variance explained (PVE) by eigenvectors ranked from least to greatest eigenvalue. Error bars represent 95% confidence bounds as calculated in North et al. (1982) assuming that each MJJ season is independent of one another.

In this analysis, we only discuss the first two eigenvectors which together account for 72.0% of the variance in MJJ season tracked evaporation from 2000 to 2023. Separately, eigenvector one accounts for 60.0% of variance and with 95% confidence, it could range from 68.7% to 51.4% of variance in our data. Eigenvector two accounts for 12.8% of variance and its confidence bounds range from 14.7% - 11.0%. By convention, eigenvector one represents the most variance in the system, but it accounts for much more variance than all of the other eigenvectors (i.e. vectors 2-28,245) combined. As seen in Figure 7, after eigenvector two, percent variance explained decreases very little with increases in each subsequent eigenvector, indicating that these eigenvectors could represent noise rather than physically meaningful variability. As such, this analysis only focuses on the first two eigenvectors and their associated principal components.

As seen in Figure 8.a, the first eigenvector (EOF1) describes a pulsing of positive and negative tracked evaporation anomalies from within Colorado. Notably, the highest evaporation contribution anomalies occur within the sink region itself, extending beyond the color bar range plotted. This eigenvector accounts for the largest portion of variance in the data, representing the dominant mode of variability among MJJ seasons from 2000 to 2023. Figure 8.b shows the normalized principal component (PC1) associated with eigenvector one. Essentially, the values in PC1 represent how much of the spatial pattern shown in EOF1 is in a given year. The MJJ season of 2023 has the strongest expression of EOF1 with over 2.5 standard deviations above the average. The dominant mode of variability that throughout 2000-2024 is expressed most intensely in the 2023 MJJ season. This further emphasizes to the extreme nature of Colorado and moisture recycling's contribution to Front Range rainfall in 2023.

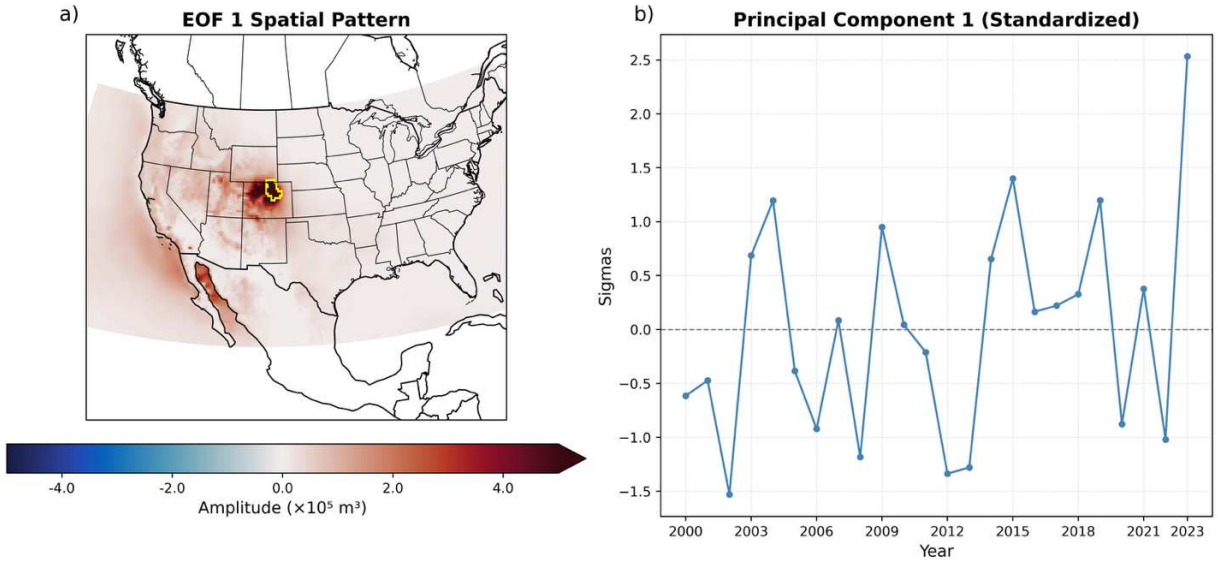


**Figure 8:** (a) Spatial pattern of the first empirical orthogonal function (EOF2) of MJJ tracked evaporation anomalies for the Front Range region (FTR) from 2000–2023. (b) Standardized principal component time series (PC1) corresponding to EOF1.

While EOF1 represents the pulsing behavior of Colorado moisture contribution, EOF2 describes a north-south dipole pattern in anomalous tracked evaporation as seen in Figure 9.a.

This spatial pattern implies that years with large negative values in PC2 (Figure 9.b) received anomalously high amounts of moisture from the Pacific Ocean and the Southwestern US and anomalously low amounts of moisture from Western US, and vice versa. The most intense tracked evaporation anomalies still reside within Colorado but also expanded to northern Utah and the Pacific Ocean. EOF2 represents 12.8% of the variance in evaporative contribution in MJJ, considerably less than EOF1, but nonetheless represents the secondary mode of variability in our data. To understand the physical basis of EOF2, more research would need to be conducted looking at the dominant synoptic environment within years with strong positive or negative PC2 values. To speculate, EOF2 could represent the movement of the subtropical jet stream altering north south moisture sources from latitudinal movement, or the variability in the North American Monsoon circulation which could lead to increased contributions from the American Southwest and Pacific Ocean. In 2023, PC2 value is only 0.2 standard deviations from the average. Since the PC2 value in 2023 is near neutral, this secondary mode of variability had little role in the 2023 MJJ season precipitation.

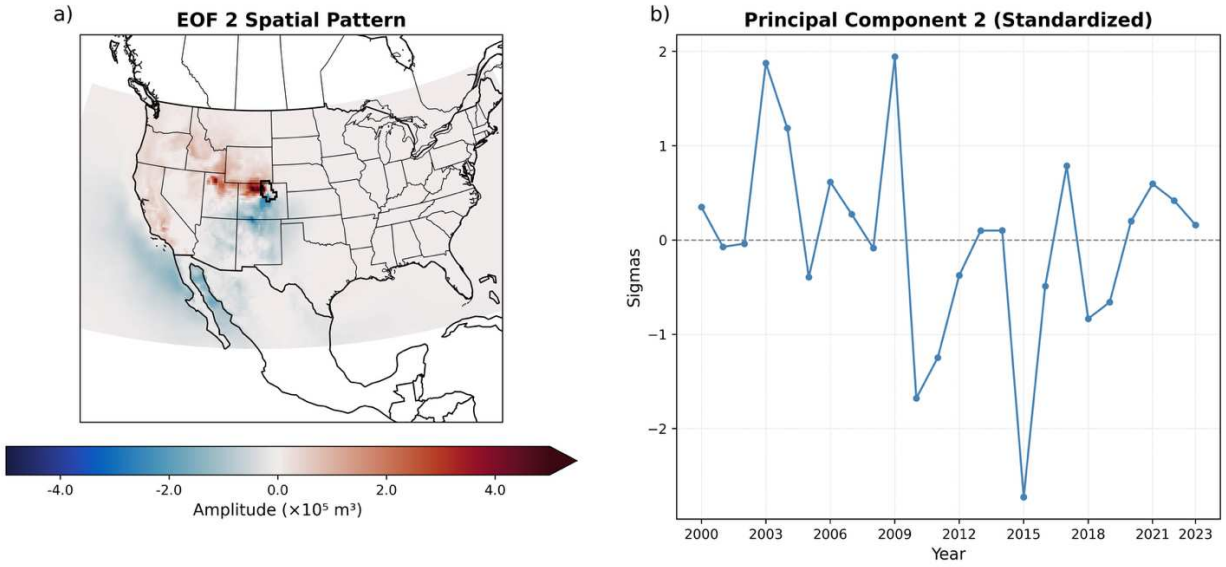


**Figure 9:** (a) Spatial pattern of the second empirical orthogonal function (EOF2) of MJJ tracked evaporation anomalies from 2000–2023. (b) Standardized principal component time series (PC2) corresponding to EOF2.

To conclude, this EOF analysis reveals the two dominant modes of moisture source variability among the past twenty-four MJJ seasons and which modes were more important in 2023. The dominant mode of variability in our dataset, EOF1, was a pulsing behavior depicting whether a given year had anomalously high or low contributions from Colorado, the Gulf of California, and the Pacific Ocean. The positive phase of EOF1 indicating increased evaporative contributions from these regions played a significant role in 2023 compared to other years. In contrast, the secondary mode of variability, EOF2, describes a dipole between northern and southern moisture sources and had much less of a role in 2023.

# CHAPTER 4: DISCUSSION AND CONCLUSION

## 4.1 Discussion

In summary, this study provides new insights into the moisture sources of the extreme precipitation in May-July of 2023 for Colorado's Front Range region. This work demonstrated that in the 2023 May, June, and July season:

1. The three dominant moisture sources were the Pacific Ocean, Western US, and Colorado, accounting for just over 66.2% of total precipitation.
2. While those regions are consistent with the dominant historical moisture sources, terrestrial sources and moisture recycling made up a greater proportion of precipitation than they have historically.
3. Moisture sources in May-July 2023 were a statistical outlier in terms of the magnitude of moisture contributed to the Front Range, forming a cluster of its own relative to the past 24 years.
4. Among the two dominant modes of variability, 2023 aligns more with a basin-wide pulsing pattern rather than a north–south dipole pattern of moisture sources.

In this section, we put these findings into a broader perspective of moisture recycling research in the Southwestern US.

Due to the recency of the 2023 events, our conclusions were more difficult to corroborate since no peer-reviewed studies had been published on these same events at the time of this writing. There is, however, literature examining moisture sources during historically wet seasons for the entire Southwestern United States (including Colorado). Based on this, we will qualitatively review how 2023 moisture sources compare broadly to sources during other wet

years. Skinner et al. (2023) found that during the wettest summers (June, July, August) in the Southwestern United States, the percent change in moisture from areas inside the region compared to normal increased by 42% and from areas outside of the Southwest, increased by 48% (Skinner et al., 2023). This could suggest that during wet years in the Southwest, there is a widespread increase in moisture content from nearly all source regions, rather than a singular anomalous import from a specific source region. Our findings indicate a similar pattern. We found that Colorado's northern Front Range received anomalously high precipitation contributions from all dominant moisture source regions. To truly understand the potential mechanism of enhanced wet season precipitation, additional modeling and analysis beyond the scope of this work would be required.

Our understanding of the northern Front Range's typical moisture sources aligns with and contrasts various findings in existing research. In a 2000 report from the Colorado Climate Center, they state that the statewide primary sources of summertime precipitation strictly come from aquatic sources such as the Pacific Ocean, the Gulf of Mexico and the Gulf of California (Mckee et al., 2000). Our results concur that the Pacific Ocean is the greatest moisture source by volume for the Front Range in May, June, and July, but we also find that the western US and Colorado itself are some of the major sources of moisture. We also affirm that aquatic sources all together make up over 50% precipitation on average and consider aquatic source regions to be more dominant source of moisture to Front Range precipitation than terrestrial sources on average (Figure 4.e).

However, our study indicates that the Gulf of California and the Gulf of Mexico are considered minor moisture sources, only making up 2.3% and 2.5% of MJJ precipitation on average. The report by Mckee does not provide quantitative estimates of moisture sources for

Colorado nor the Front Range specifically, so we are unable to directly compare results. Nonetheless, we do find general agreement in the prominence of large-scale aquatic sources, particularly the Pacific Ocean, as major contributors to MJJ precipitation in Colorado. Another likely source of discrepancy could be how we define evaporative contributions from sources. Since we define moisture sources by where precipitation last evaporated from, these regional contributions do not include moisture that initially evaporated from the Gulf of Mexico or Gulf of California but later precipitated and reevaporated again before reaching the Front Range.

Jana et al. (2018) used the Lagrangian particle tracking model, HYSPLIT, to trace the moisture trajectories of precipitation falling at a point location in Eastonville, Colorado (south of the Front Range region) from 1979–2013. This study found evidence that the dominant source of moisture in Eastern Colorado is almost exclusively land evaporation followed by modest amounts from the Gulf of California (Jana et al., 2018). In contrast, our study found that on average, terrestrial sources make up 46.2% in the Front Range which sits just north of Eastonville. Since these regions do not overlap, we expect some discrepancies in moisture sources, but due to the proximity of these areas, it is interesting that Eastonville appears to receive a much larger proportion of its rainfall from terrestrial sources.

One likely reason for this is that the Jana et al. (2018) study traced moisture backwards only for 3 days before the precipitation event. It is possible that the moisture from other sources identified in our study, such the Pacific Ocean or Atlantic Ocean, surpasses the three-day tracking limit for the HYSPLIT simulations, and so was excluded from consideration of this study. As mentioned before, water vapor has an average residence time of under nine days (van der Ent et al., 2014), so considering the Front Range's distance from oceanic bodies of water, it

is reasonable to expect water from aquatic sources to take longer than 3 days to travel to Colorado.

Our finding that terrestrial regions contributed a greater proportion of total precipitation during this specific wet year in Colorado's Front Range, is consistent with observations from other studies of wet years in the Southwest. The Skinner et al. (2023) study discussed earlier in this section found that during the wettest Springs (March, April, May), 14-18% of springtime precipitation in the Southwestern United States originated from inside the region itself (Skinner et al., 2023). Whereas during the wettest summers, recycled moisture made up 30% of Southwestern precipitation. These estimates are higher than the proportion FTR contributes to its own precipitation in May, June, and July of 2023 as shown in Figure 3.c. Given that moisture recycling is very dependent on the selected study region (van der Ent et al., 2010), it is understandable that Skinner et al.'s paper has a different proportion of moisture recycling due their study region covering a much broader area, spanning multiple states.

In terms of the possible importance of land evaporation during wet years, Erlingis et al. (2019b) suggests that in Colorado and New Mexico, summer precipitation in wetter years is prominently influenced by land surface evaporation (Erlingis et al., 2019b). Yet, more research is needed to truly understand the relationship between terrestrial sources of moisture and extreme precipitation.

Finally, we consider the results of our EOF analysis to assess dominant patterns of moisture source variability in Front Range precipitation from 2000 to 2023. As mentioned above, the lack of studies directly analyzing this event or region limits direct corroboration, so we interpret our results in the broader context of related work on large-scale moisture source variability. In Keys et al. (2014), they find that for three distinct sink regions in China, Africa,

and South America, the greatest year-to-year variability in core moisture sources is characterized by a pulsing pattern of increased or decreased evaporative contributions. This finding remains true even when using a different reanalysis dataset, MERRA (Keys et al., 2014). For the Front Range, we reach the same conclusion that interannual variability in Front Range moisture sources can best be described by pulsing of anomalous contributions from high-contributing source areas, as illustrated by EOF1 in Figure 8.a.

### 4.2 Conclusion

Focusing on some of Colorado's most populous regions, this thesis provides a comprehensive analysis on the moisture sources associated with the extremely wet May-July season of 2023. Utilizing ERA5 reanalysis data and the WAM2layers, this study provides insights into the recent evaporative origins of warm-season precipitation in Colorado's Front Range. This extraordinarily wet May-July appears to result from an anomalous increase in water vapor contributions from typical dominant source regions, with terrestrial sources and regions within Colorado playing an unexpectedly larger role than usual in the 2023 season. With these typical source regions likely driving much of the inter-annual variability in moisture sources, these findings highlight the Front Range's possible sensitivity to land-atmosphere feedback processes or changes in the evaporative fluxes of local land surface. Specifically, this work demonstrated the following key findings for the evaporative origins of the 2023 May-July season:

1. The three primary moisture sources were the Pacific Ocean, Western US, and Colorado, accounting for just over 66.2% of total precipitation.

2. While those regions are consistent with the dominant historical moisture sources, terrestrial sources and moisture recycling made up a greater proportion of precipitation than they have historically.
3. Moisture sources in May-July 2023 were a statistical outlier in terms of the magnitude of moisture contributed to the Front Range, forming a cluster of its own relative to the past 24 years.
4. Among the two dominant modes of variability, 2023 aligns more with a basin-wide pulsing pattern rather than a north–south dipole pattern of moisture sources.

### 4.3 Future Directions

Future research could benefit from a more detailed examination of the specific atmospheric pathways that moisture takes to the Front Range and the specific synoptic drivers associated with transporting water vapor. Understanding the precise transport mechanisms such as low-level jets, the North American Monsoon, and upslope flows could provide key insights into the drivers of extreme precipitation in Colorado and increase forecast ability of extreme precipitation events in Colorado. Additionally, investigating the links between large-scale teleconnections and moisture source variability would also improve our understanding of how climate modes (e.g. ENSO) regulate moisture transport to the Front Range.

Furthermore, contextualizing these results with observational datasets such as stable water isotope analysis or satellite-based water vapor observations could further validate or invalidate the moisture sources found in this study. This could also help further identify the biases and limitations of the current moisture tracking methods. Lastly, extending the analysis period beyond twenty-four years could reveal if the moisture source patterns in 2023 represent an

increasingly relevant trend or simply an anomalous outlier for the Front Range. A longer-term dataset would also strengthen the robustness of the results presented herein.

## REFERENCES


Arias, P. A., J. A. Martínez, and S. C. Vieira, 2015: Moisture sources to the 2010–2012 anomalous wet season in northern South America. *Clim Dyn*, **45**, 2861–2884, https://doi.org/10.1007/s00382-015-2511-7.

Beck, H. E., and Coauthors, 2019: Daily evaluation of 26 precipitation datasets using Stage-IV gauge-radar data for the CONUS. *Hydrol. Earth Syst. Sci.*, **23**, 207–224, https://doi.org/10.5194/hess-23-207-2019.

Bosilovich, M. G., and S. D. Schubert, 2002: Water Vapor Tracers as Diagnostics of the Regional Hydrologic Cycle. *J. Hydrometeor*, **3**, 149–165, https://doi.org/10.1175/1525-7541(2002)003<0149:WVTADO>2.0.CO;2.

Burde, G. I., and A. Zangvil, 2001: The Estimation of Regional Precipitation Recycling. Part I: Review of Recycling Models. *J. Climate*, **14**, 2497–2508, https://doi.org/10.1175/1520-0442(2001)014<2497:TEORPR>2.0.CO;2.

Ciric, D., R. Nieto, L. Losada, A. Drumond, and L. Gimeno, 2018: The Mediterranean Moisture Contribution to Climatological and Extreme Monthly Continental Precipitation. *Water*, **10**, 519, https://doi.org/10.3390/w10040519.

Cloux, S., D. Garaboa-Paz, D. Insua-Costa, G. Miguez-Macho, and V. Pérez-Muñuzuri, 2021: Extreme precipitation events in the Mediterranean area: contrasting two different models for moisture source identification. *Hydrol. Earth Syst. Sci.*, **25**, 6465–6477, https://doi.org/10.5194/hess-25-6465-2021.

Colorado Climate Center, 2024: Climate at a Glance: Rank Maps, https://climate.colostate.edu/co_cag/rank_maps.html (Accessed April 30, 2025).

Crossett, C. C., A. K. Betts, L.-A. L. Dupigny-Giroux, and A. Bomblies, 2020: Evaluation of Daily Precipitation from the ERA5 Global Reanalysis against GHCN Observations in the Northeastern United States. *Climate*, **8**, 148, https://doi.org/10.3390/cli8120148.

Dirmeyer, P. A., and K. L. Brubaker, 1999: Contrasting evaporative moisture sources during the drought of 1988 and the flood of 1993. *J. Geophys. Res.*, **104**, 19383–19397, https://doi.org/10.1029/1999JD900222.

——, ——, and T. DelSole, 2009: Import and export of atmospheric water vapor between nations. *Journal of Hydrology*, **365**, 11–22, https://doi.org/10.1016/j.jhydrol.2008.11.016.

Doesken, N. J., 2011: *Colorado's Climate: Rocky Mountain High*. Community Collaborative Rain, Hail, and Snow Network, https://media.cocorahs.org/docs/ClimateSum_CO.pdf.

——, R. A. P. Sr., and O. A. P. Bliss, 2003: *Climate of Colorado*. Colorado Climate Center and Colorado State University, https://hdl.handle.net/10217/236290.

Drumond, A., R. Nieto, E. Hernandez, and L. Gimeno, 2011: A Lagrangian analysis of the variation in moisture sources related to drier and wetter conditions in regions around the Mediterranean Basin. *Nat. Hazards Earth Syst. Sci.*, **11**, 2307–2320, https://doi.org/10.5194/nhess-11-2307-2011.

Erlingis, J. M., J. J. Gourley, and J. B. Basara, 2019a: Diagnosing Moisture Sources for Flash Floods in the United States. Part I: Kinematic Trajectories. *Journal of Hydrometeorology*, **20**, 1495–1509, https://doi.org/10.1175/JHM-D-18-0119.1.

——, ——, and ——, 2019b: Diagnosing Moisture Sources for Flash Floods in the United States. Part II: Terrestrial and Oceanic Sources of Moisture. *Journal of Hydrometeorology*, **20**, 1511–1531, https://doi.org/10.1175/JHM-D-18-0120.1.

Espinoza, J. C., J. A. Marengo, J. Ronchail, J. M. Carpio, L. N. Flores, and J. L. Guyot, 2014: The extreme 2014 flood in south-western Amazon basin: the role of tropical-subtropical South Atlantic SST gradient. *Environ. Res. Lett.*, **9**, 124007, https://doi.org/10.1088/1748-9326/9/12/124007.

Flanders Marine Institute (VLIZ), Belgium, 2018: IHO Sea Areas, version 3. Marine Data Archive, accessed 25 April 2025, https://doi.org/10.14284/323.

——, 2021: Global Oceans and Seas, version 1. Marine Data Archive, accessed 25 April 2025, https://doi.org/10.14284/542.

Gimeno, L., and Coauthors, 2020: Recent progress on the sources of continental precipitation as revealed by moisture transport analysis. *Earth-Science Reviews*, **201**, 103070, https://doi.org/10.1016/j.earscirev.2019.103070.

——, and Coauthors, 2021: The residence time of water vapour in the atmosphere. *Nat Rev Earth Environ*, **2**, 558–569, https://doi.org/10.1038/s43017-021-00181-9.

Gustafsson, M., D. Rayner, and D. Chen, 2010: Extreme rainfall events in southern Sweden: where does the moisture come from? *Tellus A: Dynamic Meteorology and Oceanography*, **62**, 605, https://doi.org/10.1111/j.1600-0870.2010.00456.x.

Hersbach, H., and Coauthors, 2020: The ERA5 global reanalysis. *Quart J Royal Meteoro Soc*, **146**, 1999–2049, https://doi.org/10.1002/qj.3803.

Hu, H., and F. Dominguez, 2015: Evaluation of Oceanic and Terrestrial Sources of Moisture for the North American Monsoon Using Numerical Models and Precipitation Stable Isotopes. *Journal of Hydrometeorology*, **16**, 19–35, https://doi.org/10.1175/JHM-D-14-0073.1.

Jana, S., B. Rajagopalan, M. A. Alexander, and A. J. Ray, 2018: Understanding the Dominant Sources and Tracks of Moisture for Summer Rainfall in the Southwest United States. *JGR Atmospheres*, **123**, 4850–4870, https://doi.org/10.1029/2017JD027652.

Kalverla, P., I. Benedict, C. Weijenborg, and R. J. Van Der Ent, 2024: Atmospheric moisture tracking with WAM2layers v3, https://doi.org/10.5194/egusphere-2024-3401.

Keys, P. W., R. J. Van Der Ent, L. J. Gordon, H. Hoff, R. Nikoli, and H. H. G. Savenije, 2012: Analyzing precipitationsheds to understand the vulnerability of rainfall dependent regions. *Biogeosciences*, **9**, 733–746, https://doi.org/10.5194/bg-9-733-2012.

——, E. A. Barnes, R. J. Van Der Ent, and L. J. Gordon, 2014: Variability of moisture recycling using a precipitationshed framework. *Hydrol. Earth Syst. Sci.*, **18**, 3937–3950, https://doi.org/10.5194/hess-18-3937-2014.

Keys, P. W., L. Wang-Erlandsson, and L. J. Gordon, 2016: Revealing Invisible Water: Moisture Recycling as an Ecosystem Service. *PLoS ONE*, **11**, e0151993, https://doi.org/10.1371/journal.pone.0151993.

Kim, S., and F. Dominguez, 2023: Warm Season Extreme Flood Events in the Midwestern US—Sources of Moisture and Physical Mechanisms. *JGR Atmospheres*, **128**, e2022JD038208, https://doi.org/10.1029/2022JD038208.

Kirk, J. P., and T. W. Schmidlin, 2018: Moisture transport associated with large precipitation events in the Upper Colorado River Basin. *Intl Journal of Climatology*, **38**, 5323–5338, https://doi.org/10.1002/joc.5734.

Knoche, H. R., and H. Kunstmann, 2013: Tracking atmospheric water pathways by direct evaporation tagging: A case study for West Africa. *JGR Atmospheres*, **118**, https://doi.org/10.1002/2013JD019976.

Liu, X., C. Guo, J. Zhang, Y. Liu, M. Xiao, Y. Wu, B. Li, and T. Zhao, 2024: Moisture sources of precipitation over the Pearl River Basin in South China. *Intl Journal of Climatology*, **44**, 2160–2173, https://doi.org/10.1002/joc.8447.

Liu, Y., and Coauthors, 2021: Moisture source variations for summer rainfall in different intensity classes over Huaihe River Valley, China. *Clim Dyn*, **57**, 1121–1133, https://doi.org/10.1007/s00382-021-05762-4.

Lloyd, S., 1982: Least squares quantization in PCM. *IEEE Trans. Inform. Theory*, **28**, 129–137, https://doi.org/10.1109/TIT.1982.1056489.

Marengo, J. A., L. M. Alves, W. R. Soares, D. A. Rodriguez, H. Camargo, M. P. Riveros, and A. D. Pabló, 2013: Two Contrasting Severe Seasonal Extremes in Tropical South America in 2012: Flood in Amazonia and Drought in Northeast Brazil. *Journal of Climate*, **26**, 9137–9154, https://doi.org/10.1175/JCLI-D-12-00642.1.

McKee, T., N. J. Doesken, J. Kliest, C. J. Shrier, and W. P. Stanton, 2000: *A History of Drought in Colorado: Lessons Learned and What Lies Ahead*. Colorado State University and Colorado Water Resources Research Institute, http://hdl.handle.net/10217/4216.

North, G. R., T. L. Bell, R. F. Cahalan, and F. J. Moeng, 1982: Sampling Errors in the Estimation of Empirical Orthogonal Functions. *Mon. Wea. Rev.*, **110**, 699–706, https://doi.org/10.1175/1520-0493(1982)110<0699:SEITEO>2.0.CO;2.

Pedregosa, F., and Coauthors, 2012: Scikit-learn: Machine Learning in Python, https://doi.org/10.48550/ARXIV.1201.0490.

Pinto, J. G., S. Ulbrich, A. Parodi, R. Rudari, G. Boni, and U. Ulbrich, 2013: Identification and ranking of extraordinary rainfall events over Northwest Italy: The role of Atlantic moisture. *JGR Atmospheres*, **118**, 2085–2097, https://doi.org/10.1002/jgrd.50179.

Rapolaki, R. S., R. C. Blamey, J. C. Hermes, and C. J. C. Reason, 2021: Moisture sources and transport during an extreme rainfall event over the Limpopo River Basin, southern Africa. *Atmospheric Research*, **264**, 105849, https://doi.org/10.1016/j.atmosres.2021.105849.

Rios-Entenza, A., and G. Miguez-Macho, 2014: Moisture recycling and the maximum of precipitation in spring in the Iberian Peninsula. *Clim Dyn*, **42**, 3207–3231, https://doi.org/10.1007/s00382-013-1971-x.

Schumacher, R., R. Bolinger, and J. Lukas, 2024: Development of Alternate Climate Divisions for Colorado Based on Gridded Data. *JoASC*, **2024**, 1–9, https://doi.org/10.46275/JOASC.2024.06.002.

Skinner, C. B., T. S. Harrington, M. Barlow, and L. Agel, 2023: The contribution of precipitation recycling to North American wet and dry precipitation extremes. *Environ. Res.: Climate*, **2**, 045010, https://doi.org/10.1088/2752-5295/acffea.

Syakur, M. A., B. K. Khotimah, E. M. S. Rochman, and B. D. Satoto, 2018: Integration K-Means Clustering Method and Elbow Method For Identification of The Best Customer Profile Cluster. *IOP Conf. Ser.: Mater. Sci. Eng.*, **336**, 012017, https://doi.org/10.1088/1757-899X/336/1/012017.

Tan, X., T. Y. Gan, and Y. D. Chen, 2018: Moisture sources and pathways associated with the spatial variability of seasonal extreme precipitation over Canada. *Clim Dyn*, **50**, 629–640, https://doi.org/10.1007/s00382-017-3630-0.

Tarek, M., F. P. Brissette, and R. Arsenault, 2020: Evaluation of the ERA5 reanalysis as a potential reference dataset for hydrological modelling over North America. *Hydrol. Earth Syst. Sci.*, **24**, 2527–2544, https://doi.org/10.5194/hess-24-2527-2020.

Tuinenburg, O. A., and A. Staal, 2020: Tracking the global flows of atmospheric moisture and associated uncertainties. *Hydrol. Earth Syst. Sci.*, **24**, 2419–2435, https://doi.org/10.5194/hess-24-2419-2020.

Tuinenburg, O. A., R. W. A. Hutjes, and P. Kabat, 2012: The fate of evaporated water from the Ganges basin. *J. Geophys. Res.*, **117**, 2011JD016221, https://doi.org/10.1029/2011JD016221.

van der Ent, R. J., and O. A. Tuinenburg, 2017: The residence time of water in the atmosphere revisited. *Hydrol. Earth Syst. Sci.*, **21**, 779–790, https://doi.org/10.5194/hess-21-779-2017.

van der Ent, R. J., H. H. G. Savenije, B. Schaefli, and S. C. Steele-Dunne, 2010: Origin and fate of atmospheric moisture over continents. *Water Resources Research*, **46**, 2010WR009127, https://doi.org/10.1029/2010WR009127.

van der Ent, R. J., L. Wang-Erlandsson, P. W. Keys, and H. H. G. Savenije, 2014: Contrasting roles of interception and transpiration in the hydrological cycle – Part 2: Moisture recycling. *Earth Syst. Dynam.*, **5**, 471–489, https://doi.org/10.5194/esd-5-471-2014.

van der Ent, R. J., I. B. Benedict, C. Weijenborg, T. Cömert, N. van de Koppel, L. Guo, V. de Feiter, and P. Kalverla, 2023: WAM2layers, https://doi.org/10.5281/ZENODO.8172344.

Wei, J., P. A. Dirmeyer, D. Wisser, M. G. Bosilovich, and D. M. Mocko, 2013: Where Does the Irrigation Water Go? An Estimate of the Contribution of Irrigation to Precipitation Using MERRA. *Journal of Hydrometeorology*, **14**, 275–289, https://doi.org/10.1175/JHM-D-12-079.1.

Yang, Z., Y. Qian, P. Xue, J. Wang, T. C. Chakraborty, W. J. Pringle, J. Li, and X. Chen, 2023: Moisture Sources of Precipitation in the Great Lakes Region: Climatology and Recent Changes. *Geophysical Research Letters*, **50**, e2022GL100682, https://doi.org/10.1029/2022GL100682.

Zhang, C., Q. Tang, Y. Zhao, D. Chen, J. Huang, Y. Liu, and X. Zhang, 2024: Moisture source differences between the 2020 and 1998 super Meiyu-flood events in the Yangtze River Valley. *Weather and Climate Extremes*, **43**, 100644, https://doi.org/10.1016/j.wace.2024.100644.

Zhang, X., and Coauthors, 2023: Examining moisture contribution for precipitation in response to climate change and anthropogenic factors in Hengduan Mountain Region, China. *Journal of Hydrology*, **620**, 129562, https://doi.org/10.1016/j.jhydrol.2023.129562.

Zhao, Y., X. Xu, T. Zhao, H. Xu, F. Mao, H. Sun, and Y. Wang, 2016: Extreme precipitation events in East China and associated moisture transport pathways. *Sci. China Earth Sci.*, **59**, 1854–1872, https://doi.org/10.1007/s11430-016-5315-7.

APPENDIX A: SUPPLEMENTAL FIGURES AND ANALYSIS

## A.1 Source and Sink Region Maps

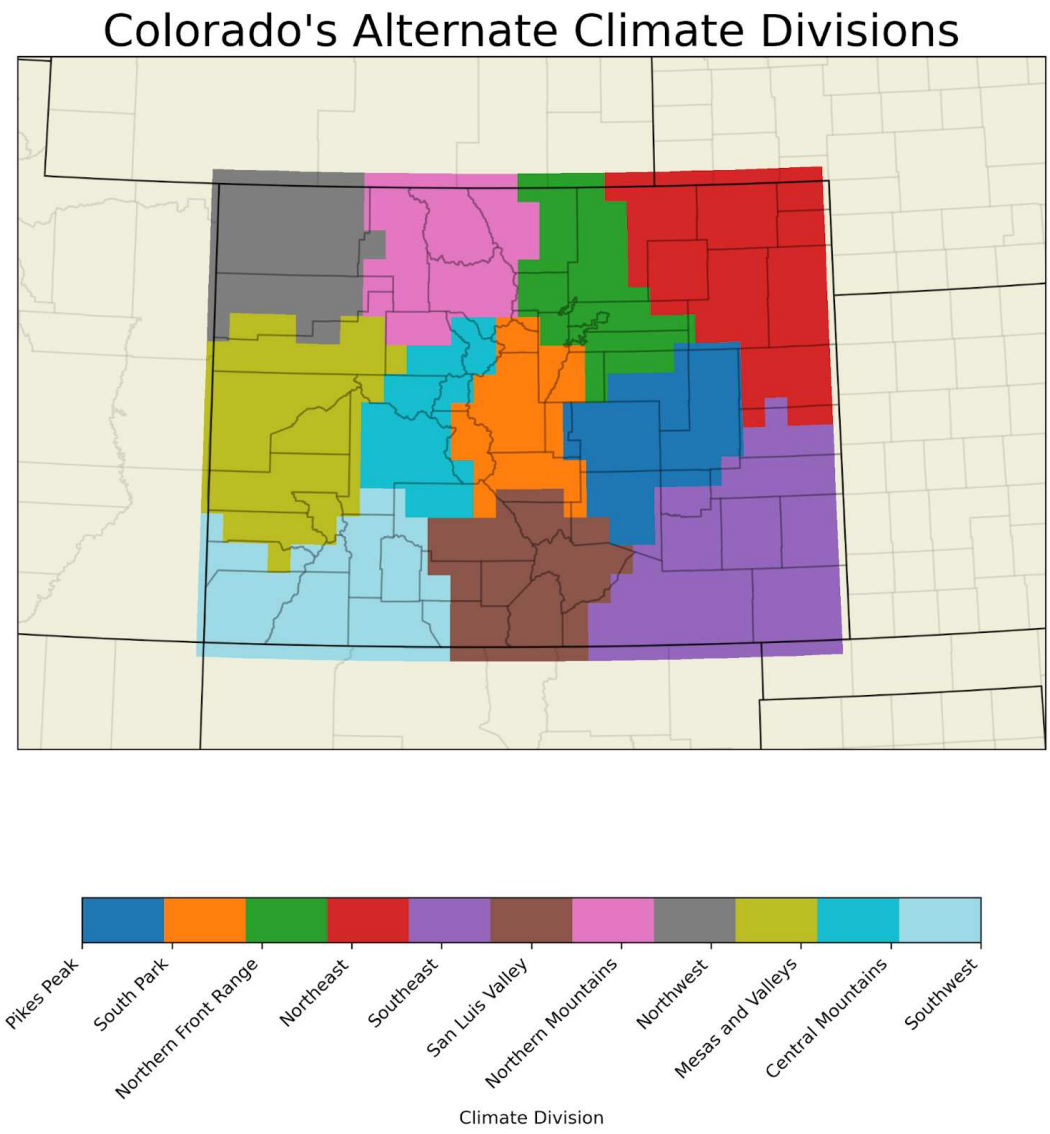


**Figure A.1.1:** Colorado's Alternate Climate Divisions described in Schumacher et al. (2024) adapted to a 0.25°x0.25° latitude longitude grid. State and county boundaries are marked in black and grey.

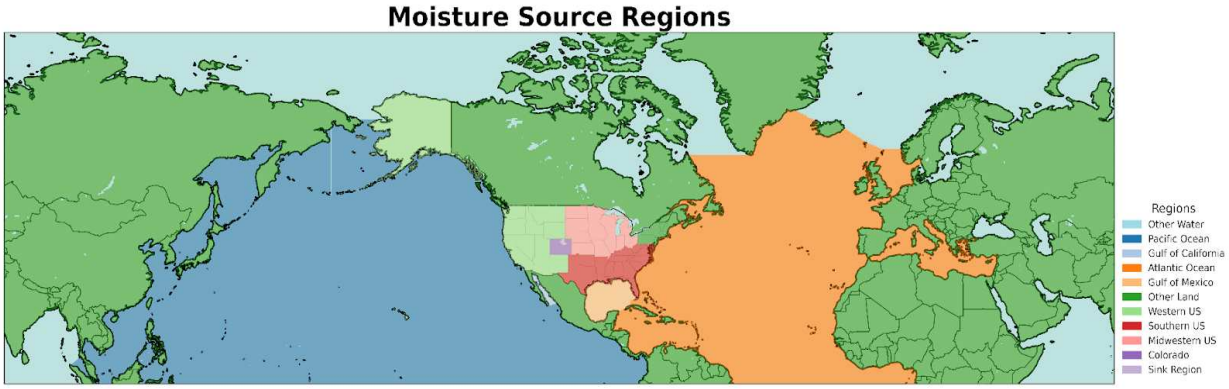


**Figure A.1.2:** Classification of moisture source regions. Broader ocean areas follow the Global Oceans and Seas dataset (Flanders Marine Institute, 2021), and suboceanic regions, including the Gulf of Mexico and Gulf of California, are defined using International Hydrographic Organization boundaries (Flanders Marine Institute, 2018). Land-based regions are based on the U.S. Census Bureau regional divisions. The sink region shown here is the Front Range, but changes depending on the sink region for each analysis.

## A.2 Domain Sensitivity Analysis

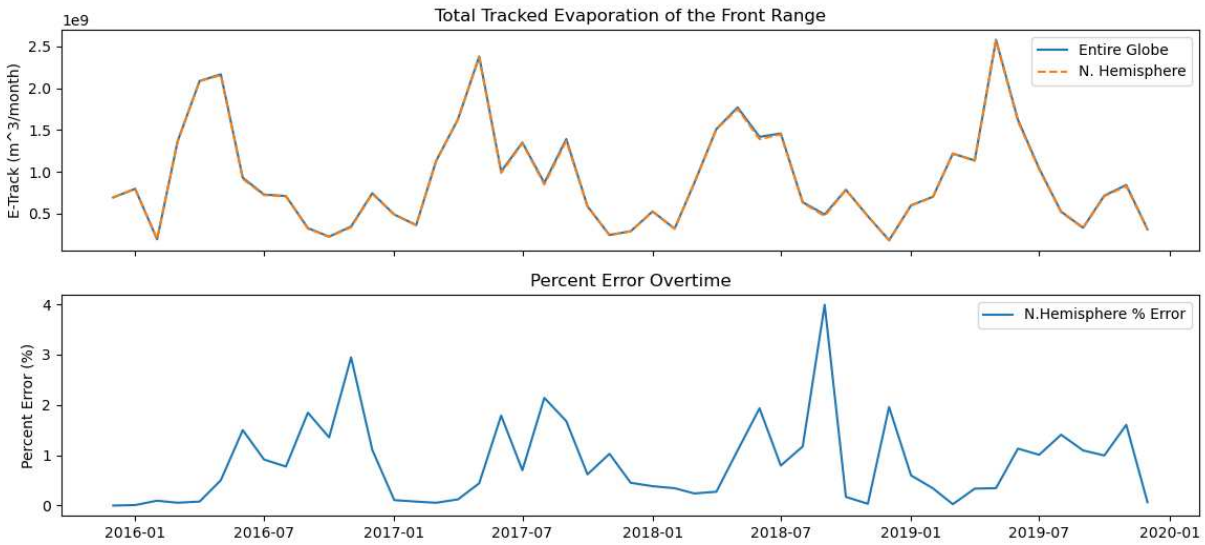


**Figure A.2.1:** Sensitivity analysis comparing the monthly spatially sumed tracked evaporation between WAM2layer runs with different latitude-longitude constraints. The global run tracks evaporation from regions within 80°S to 80°N latitude whereas the northern hemisphere runs from 0° to 80°N latitude.

## A.3 Eastern Plains Region Analysis

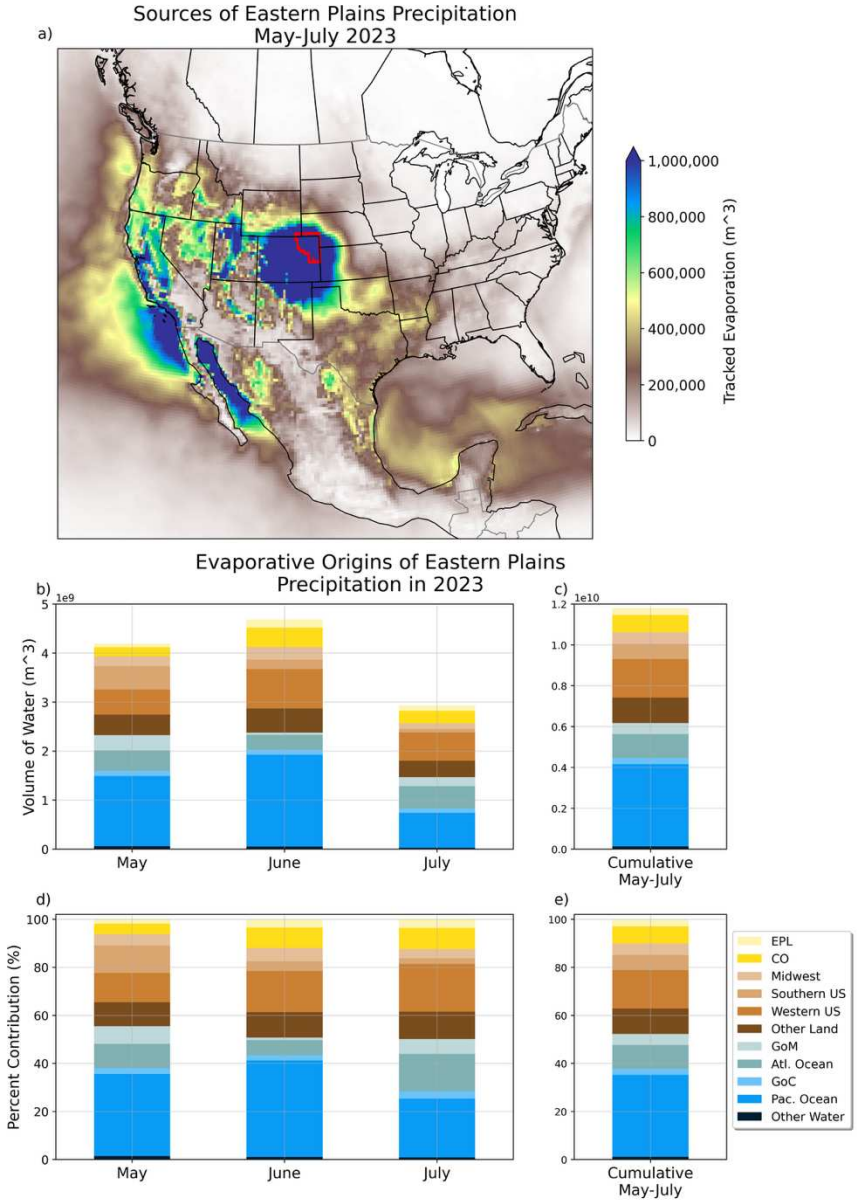


**Figure A.3.1:** a), b), c), d), e) Spatial and monthly variation in moisture sources of Eastern Plains (EPL) precipitation in May, June, and July of 2023. a) Map of evaporative sources of EPL precipitation accumulating from May through July of 2023. b) Monthly regional contribution to the EPL in volume of water vapor ($m^3$). c) Cumulative regional evaporative contribution across May, June and July of 2023 to EPL precipitation in volume of water vapor ($m^3$). d) Monthly regional evaporative contribution as a percent of total monthly evaporative contribution. e) Cumulative regional contribution as a percent of total monthly evaporative contribution. Sink region outlined in red. Note, y-axis ranges in b) and c) span a larger array of values since this region received more precipitation than the Front Range.

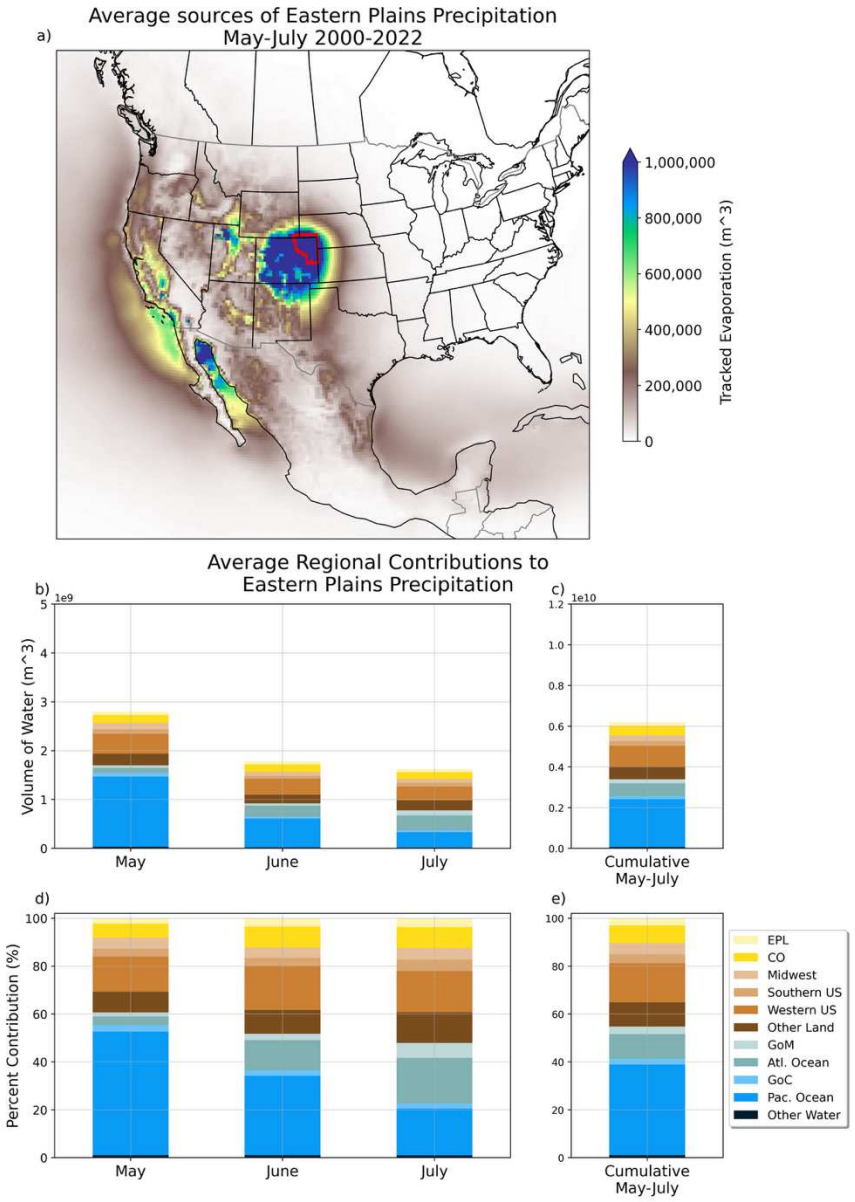


**Figure A.3.2:** (a), (b), (c) Spatial and monthly variation of Eastern Plains (EPL) moisture sources averaged from 2000-2022. (a) Map of average tracked evaporation accumulating from May through July. (b) Average monthly regional contributions to the EPL in volume of water vapor ($m^3$). (c) Average cumulative regional contribution across May, June and July to FTR precipitation in volume of water vapor ($m^3$). Note, y-axis ranges in b) and c) span a larger array of values since this region received more precipitation than the Front Range.

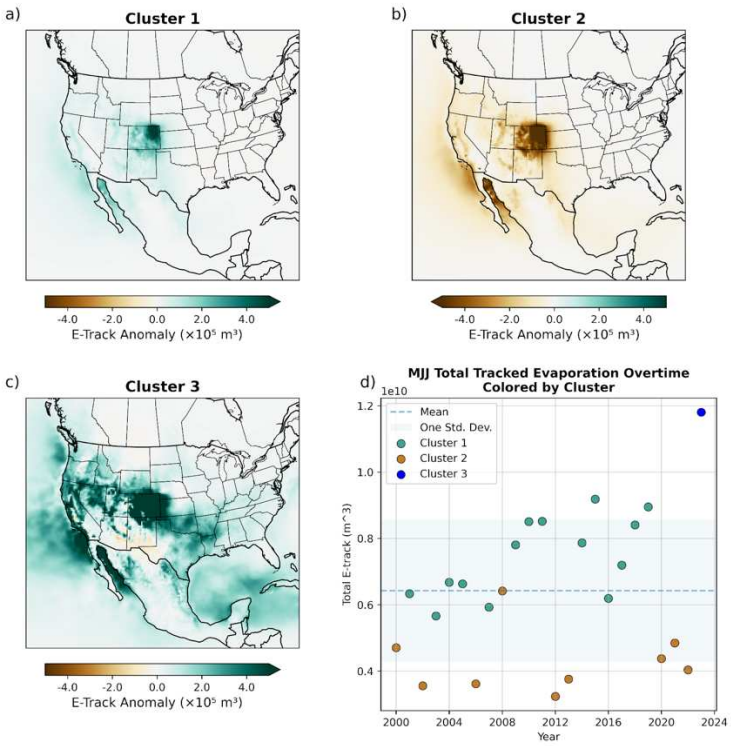


**Figure A.3.3:** Spatiotemporal patterns of MJJ evaporation anomalies of Eastern Plains (EPL) precipitation from k-means Clustering. (a), (b), (c) Cluster average MJJ moisture contribution. (d) MJJ total precipitation (spatially summed e-track) overtime colored by the assigned cluster.

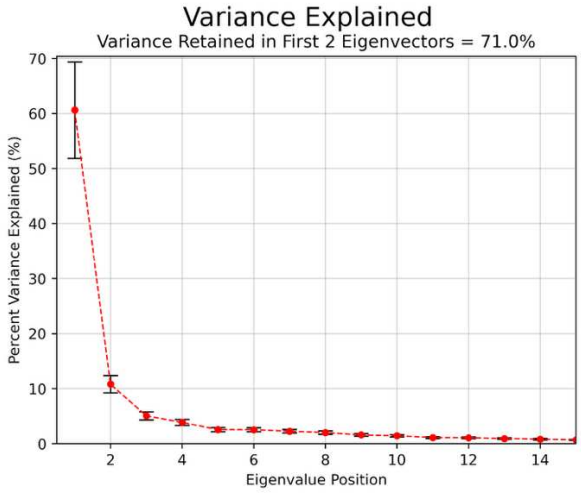


**Figure A.3.4:** Results from EOF analysis on the Eastern Plains region (EPL). Percent variance explained (PVE) by eigenvectors ranked from least to greatest eigenvalue. Error bars represent 95% confidence bounds as calculated in North et al. (1982) assuming that each MJJ season is independent of one another.

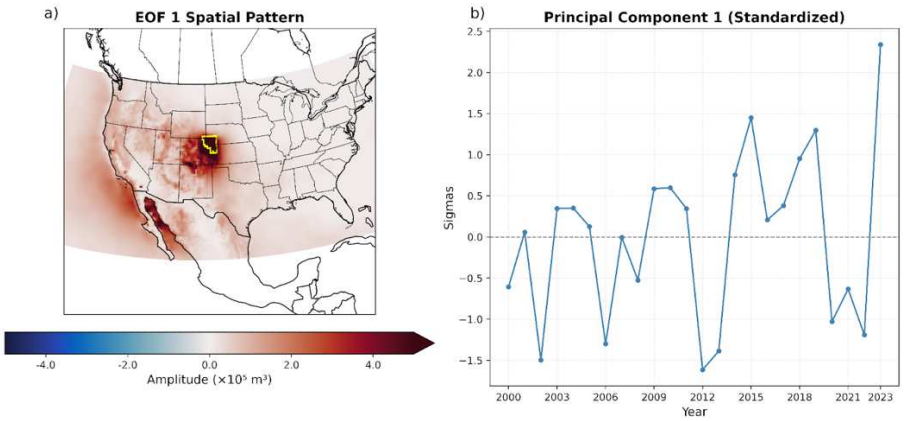


**Figure A.3.5:** (a) Spatial pattern of the first empirical orthogonal function (EOF1) of MJJ tracked evaporation anomalies for the Eastern Plains region (EPL) from 2000–2023. (b) Standardized principal component time series (PC1) corresponding to EOF1. Sink region marked in yellow.

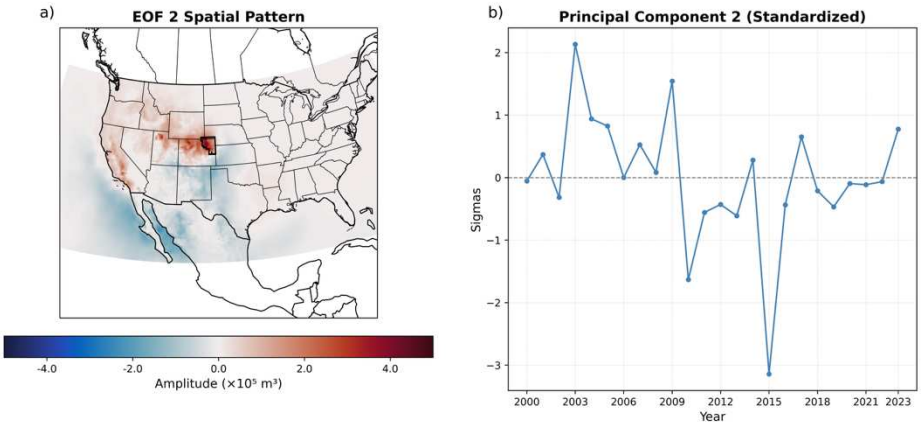


**Figure A.3.6:** (a) Spatial pattern of the first empirical orthogonal function (EOF2) of MJJ tracked evaporation anomalies for the Eastern Plains region (EPL) from 2000–2023. (b) Standardized principal component time series (PC2) corresponding to EOF2. Sink region outlined in black.

## A.4 Arkansas Basin Region Analysis

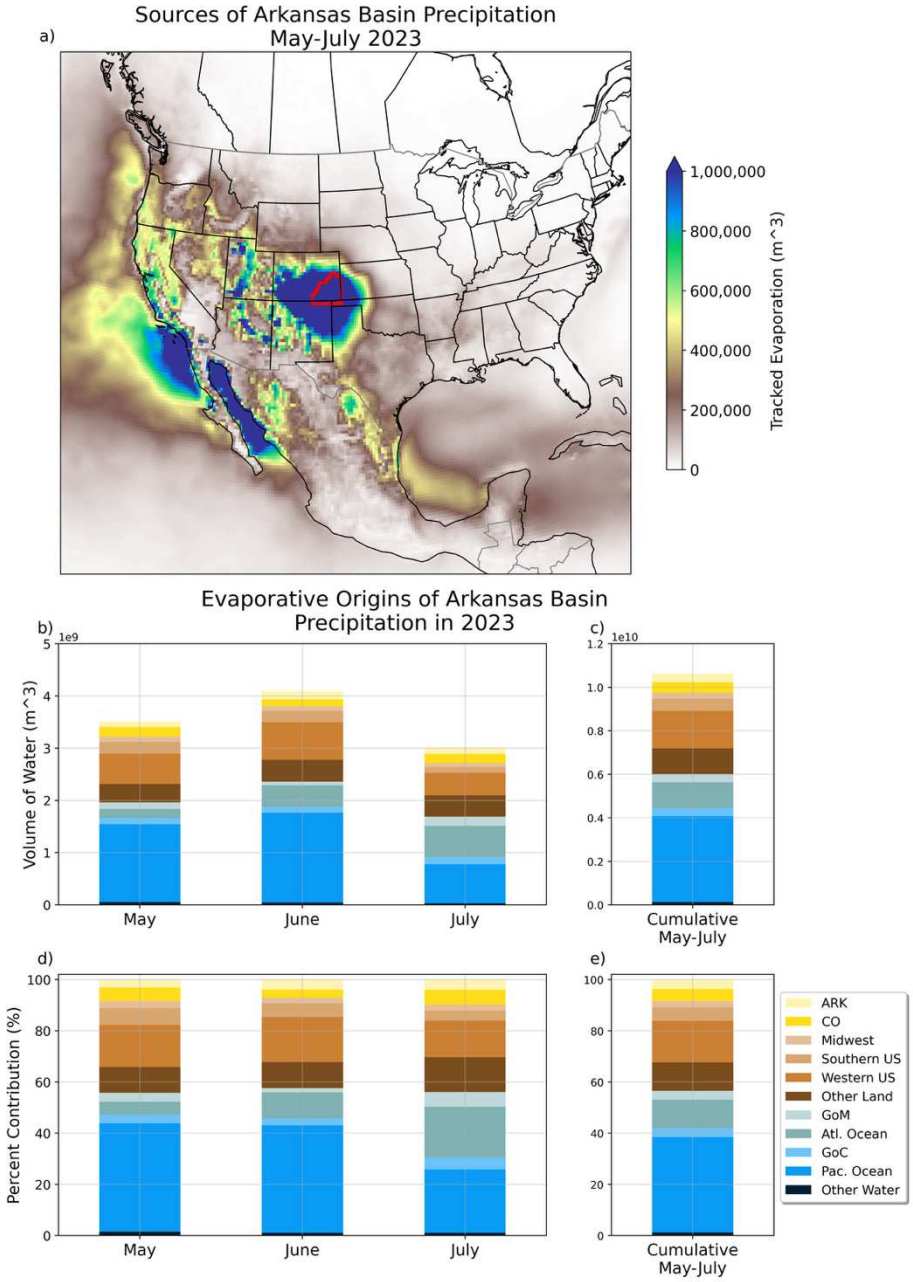


**Figure A.4.1:** a), b), c), d), e) Spatial and monthly variation in moisture sources of Arkansas Basin region (ARK) precipitation in May, June, and July of 2023. a) Map of evaporative sources of ARK precipitation accumulating from May through July of 2023. b) Monthly regional contribution to the ARK in volume of water vapor ($m^3$). c) Cumulative regional evaporative contribution across May, June and July of 2023 to ARK precipitation in volume of water vapor ($m^3$). d) Monthly regional evaporative contribution as a percent of total monthly evaporative contribution. e) Cumulative regional contribution as a percent of total monthly evaporative contribution. Sink region outlined in red. Note, y-axis ranges in b) and c) span a larger array of values since this region received more precipitation than the Front Range.

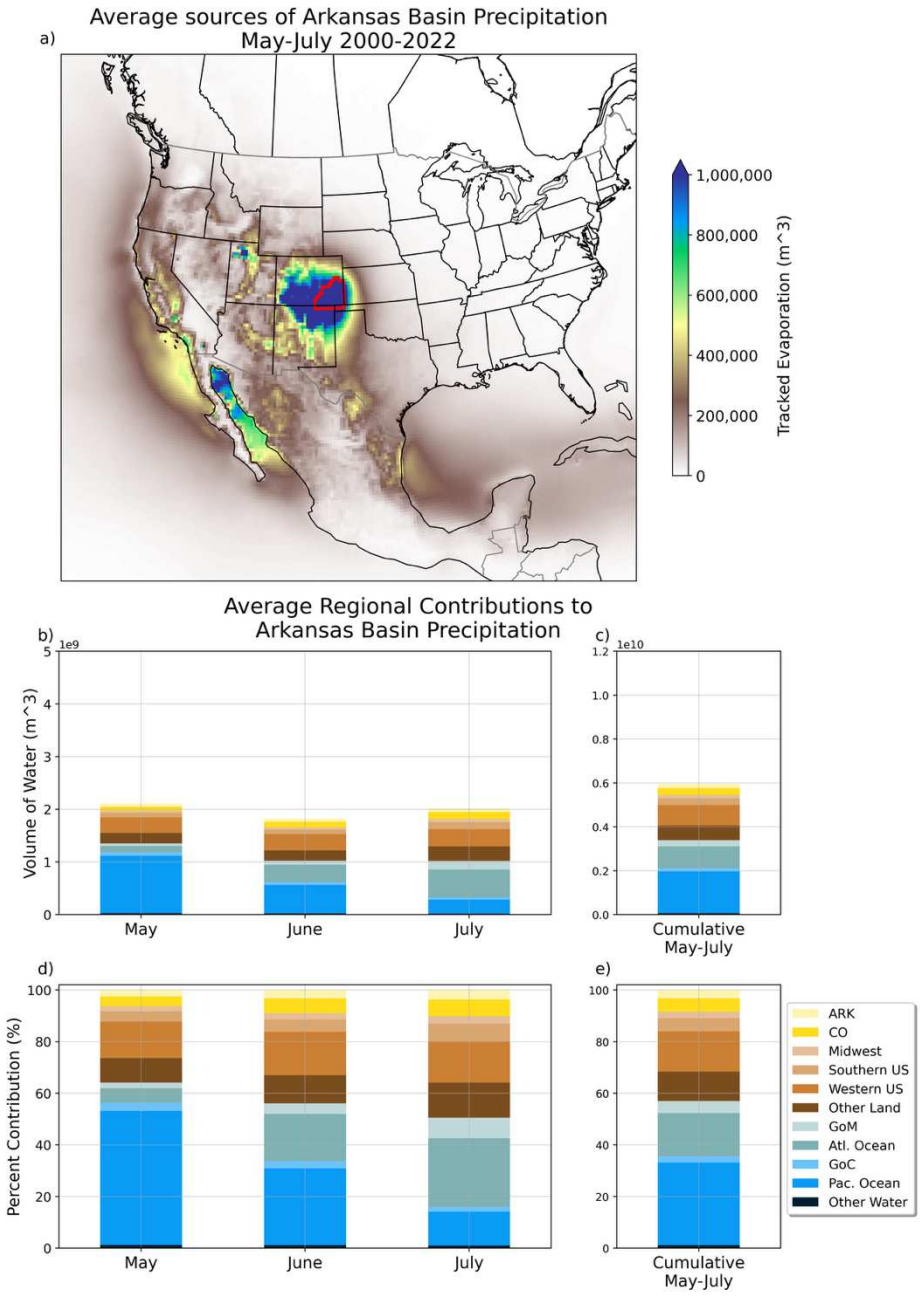


**Figure A.4.2:** (a), (b), (c) Spatial and monthly variation of Arkansas Basin (ARK) moisture sources averaged from 2000-2022. (a) Map of average tracked evaporation accumulating from May through July. (b) Average monthly regional contributions to the ARK in volume of water vapor ($m^3$). (c) Average cumulative regional contribution across May, June and July to ARK precipitation in volume of water vapor ($m^3$). Sink region outlined in red. Note, y-axis ranges in b) and c) span a larger array of values since this region received more precipitation than the Front Range.

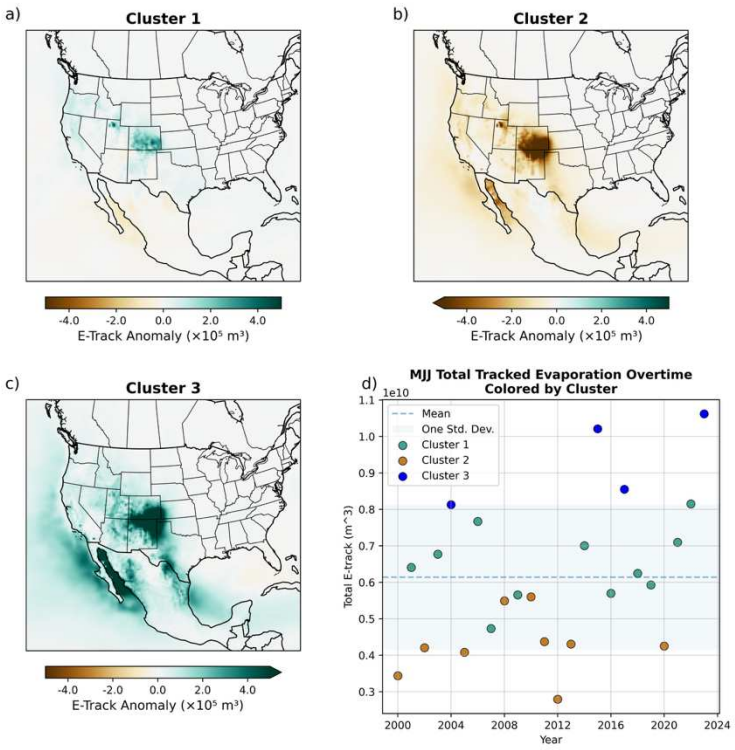


**Figure A.4.3:** Spatiotemporal patterns of MJJ evaporation anomalies of Arkansas Basin (ARK) precipitation from k-means Clustering. (a), (b), (c) Cluster average MJJ moisture contribution. (d) MJJ total precipitation (spatially summed e-track) overtime colored by the assigned cluster.

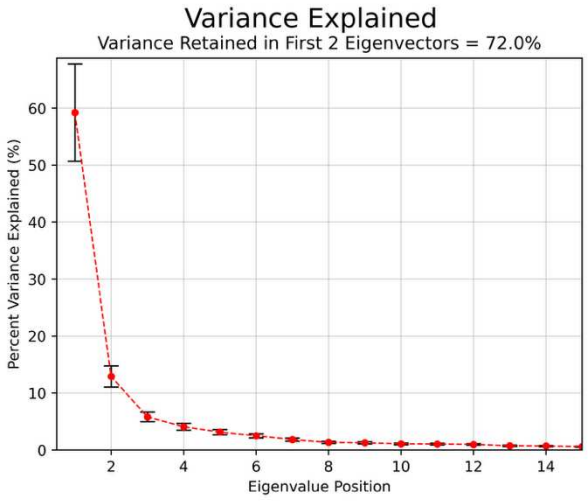


**Figure A.4.4:** Results from EOF analysis on the Arkansas Basin region (ARK). Percent variance explained (PVE) by eigenvectors ranked from least to greatest eigenvalue. Error bars represent 95% confidence bounds as calculated in North et al. (1982) assuming that each MJJ season is independent of one another.

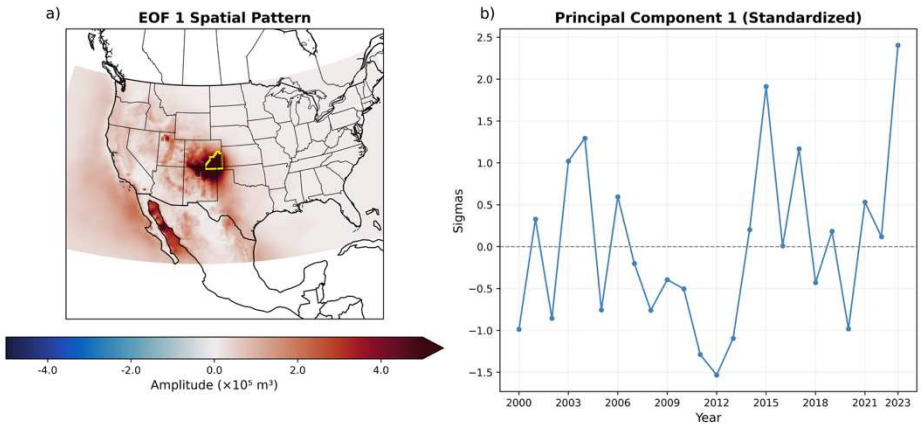


**Figure A.4.5:** (a) Spatial pattern of the first empirical orthogonal function (EOF1) of MJJ tracked evaporation anomalies for the Arkansas Basin region (ARK) from 2000–2023. (b) Standardized principal component time series (PC1) corresponding to EOF1. Sink region marked in yellow.

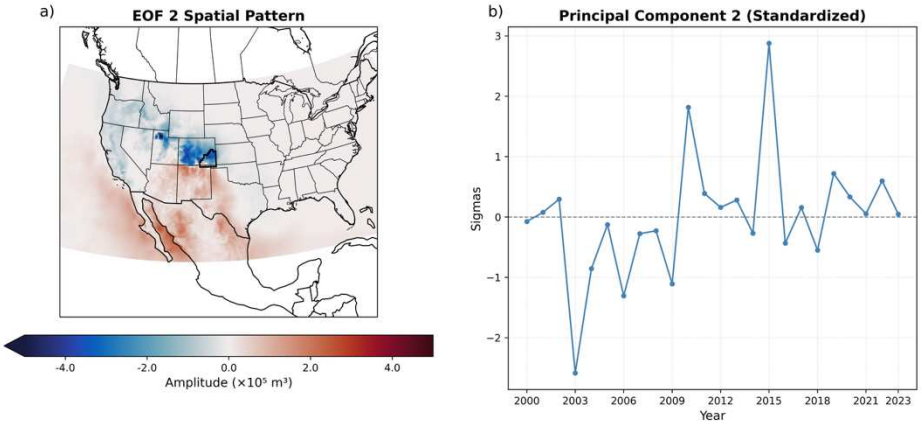


**Figure A.4.6:** (a) Spatial pattern of the first empirical orthogonal function (EOF2) of MJJ tracked evaporation anomalies for the Arkansas Basin region (ARK) from 2000–2023. (b) Standardized principal component time series (PC2) corresponding to EOF2. Sink region outlined in black.

## A.5 High Mountain Valley Region Analysis

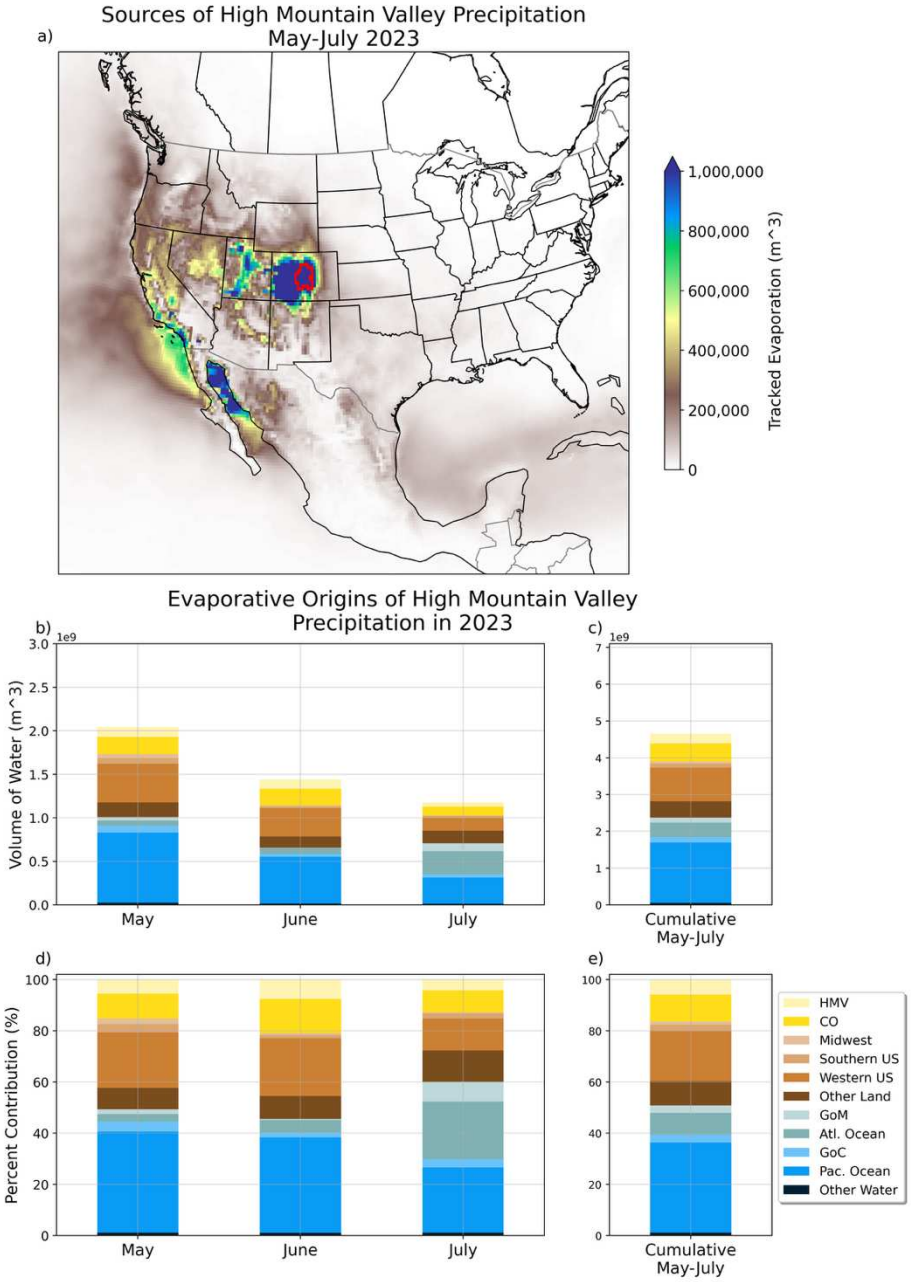


**Figure A.5.1:** a), b), c), d), e) Spatial and monthly variation in moisture sources of High Mountain Valley region (HMV) precipitation in May, June, and July of 2023. a) Map of evaporative sources of HMV precipitation accumulating from May through July of 2023. b) Monthly regional contribution to the HMV in volume of water vapor ($m^3$). c) Cumulative regional evaporative contribution across May, June and July of 2023 to HMV precipitation in volume of water vapor ($m^3$). d) Monthly regional evaporative contribution as a percent of total monthly evaporative contribution. e) Cumulative regional contribution as a percent of total monthly evaporative contribution. Sink region outlined in red.

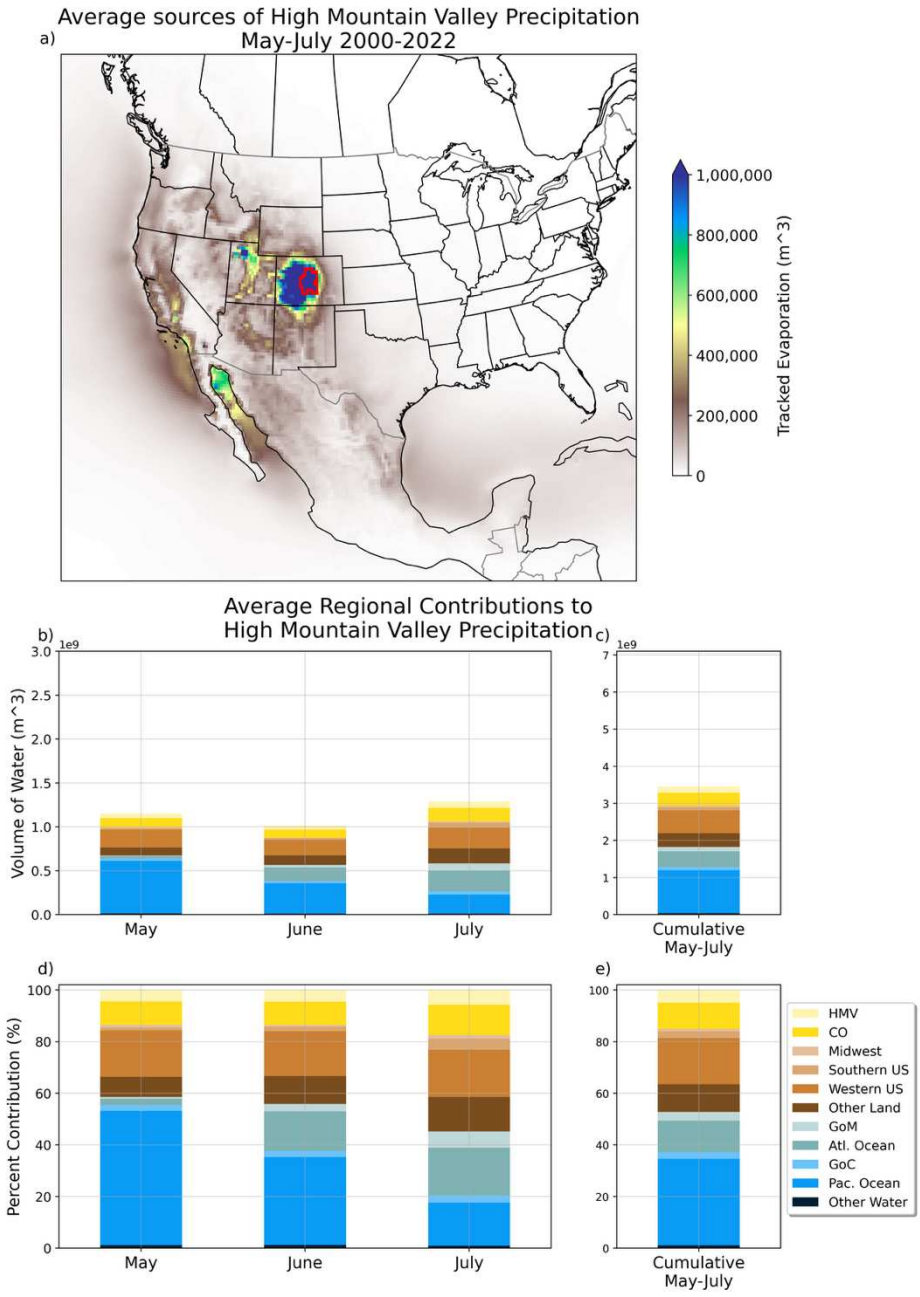


**Figure A.5.2:** (a), (b), (c) Spatial and monthly variation of High Mountain Valley (HMV) moisture sources averaged from 2000-2022. (a) Map of average tracked evaporation accumulating from May through July. (b) Average monthly regional contributions to the HMV in volume of water vapor ($m^3$). (c) Average cumulative regional contribution across May, June and July to HMV precipitation in volume of water vapor ($m^3$). Sink region outlined in red.

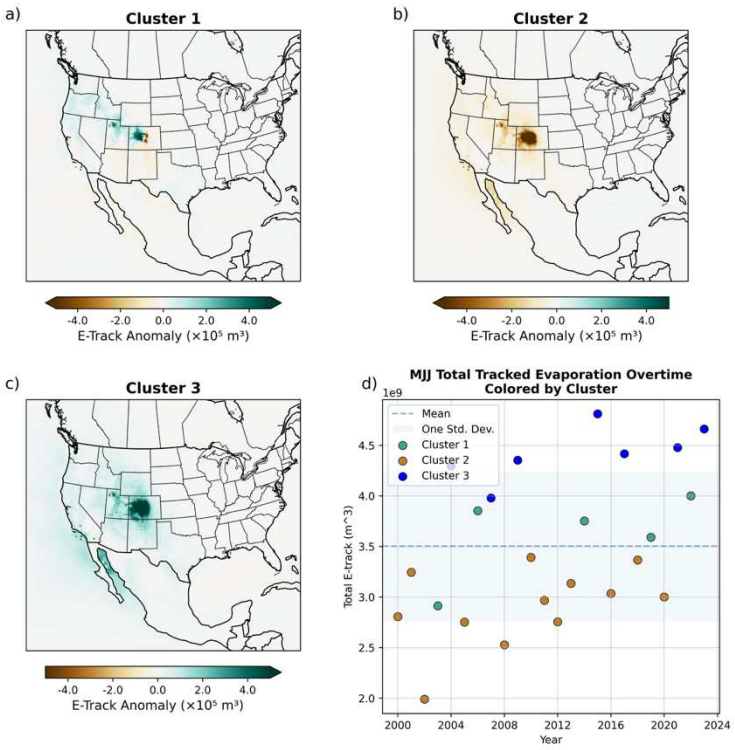


**Figure A.5.3:** Spatiotemporal patterns of MJJ evaporation anomalies of High Mountain Valley (HMV) precipitation from k-means Clustering. (a), (b), (c) Cluster average MJJ moisture contribution. (d) MJJ total precipitation (spatially summed e-track) overtime colored by the assigned cluster.

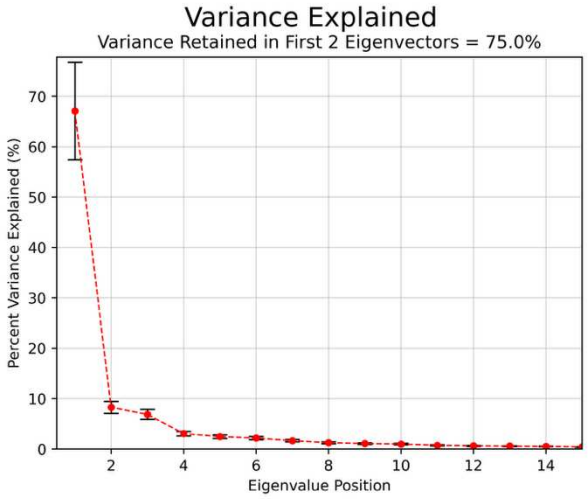


**Figure A.5.4:** Results from EOF analysis on the High Mountain Valley region (HMV). Percent variance explained (PVE) by eigenvectors ranked from least to greatest eigenvalue. Error bars represent 95% confidence bounds as calculated in North et al. (1982) assuming that each MJJ season is independent of one another.

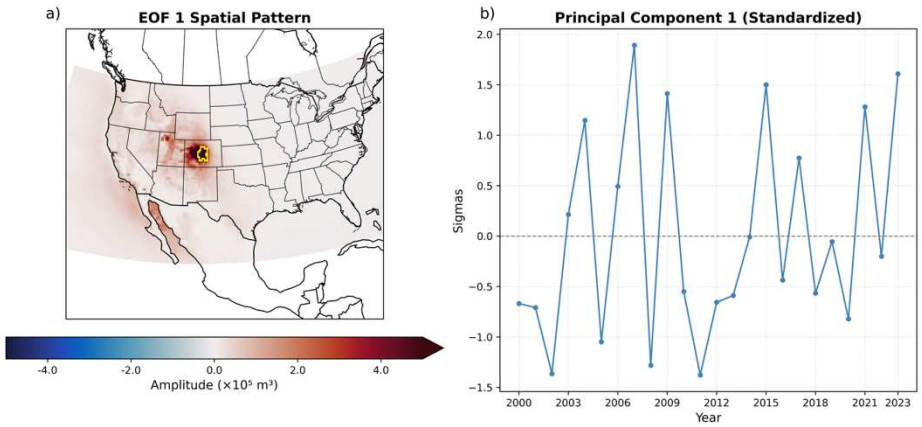


**Figure A.5.5:** (a) Spatial pattern of the first empirical orthogonal function (EOF1) of MJJ tracked evaporation anomalies for the High Mountain Valley region (HMV) from 2000–2023. (b) Standardized principal component time series (PC1) corresponding to EOF1. Sink region marked in yellow.

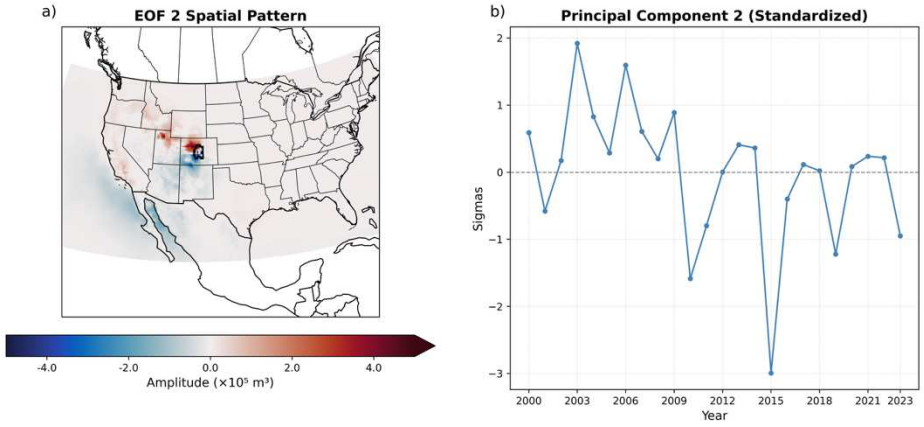


**Figure A.5.6:** (a) Spatial pattern of the first empirical orthogonal function (EOF2) of MJJ tracked evaporation anomalies for the High Mountain Valley region (HMV) from 2000–2023. (b) Standardized principal component time series (PC2) corresponding to EOF2. Sink region outlined in black.

## A.6 Pikes Peak Region Analysis

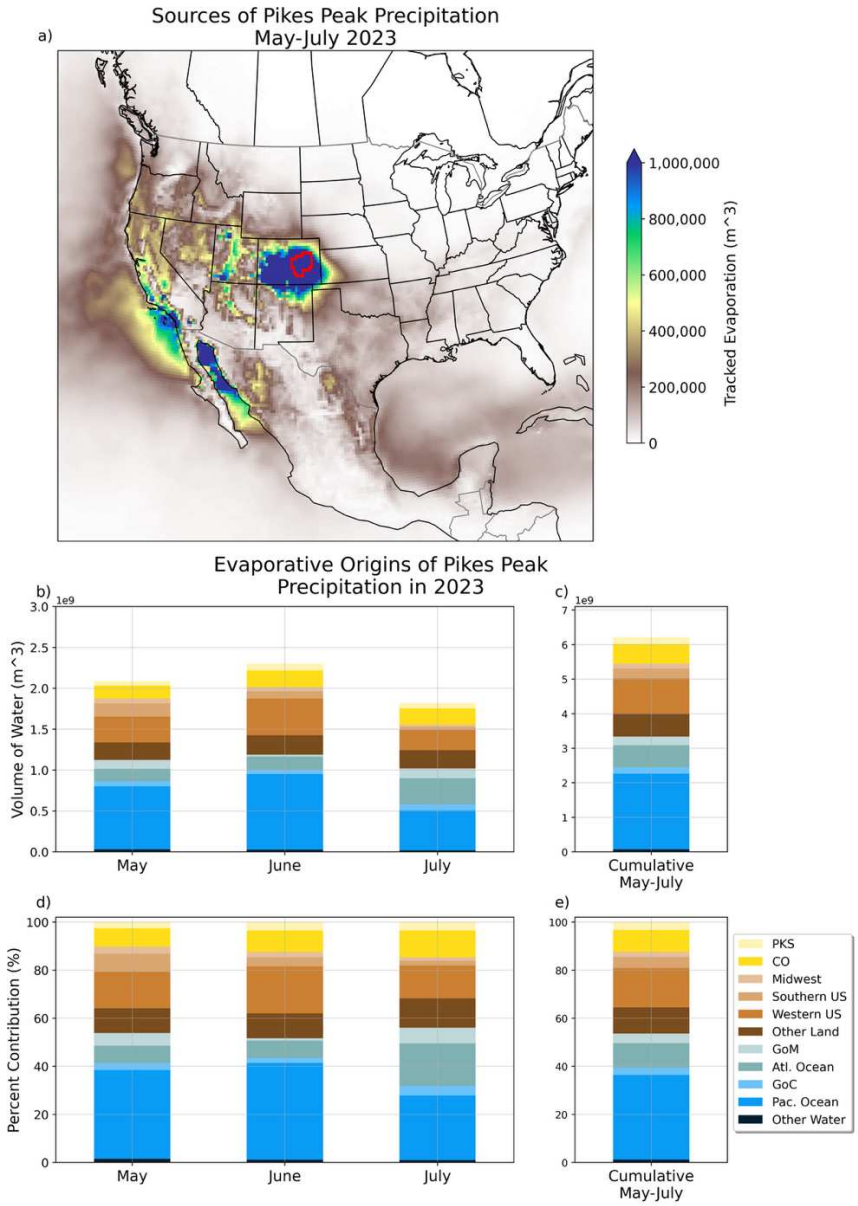


**Figure A.6.1:** a), b), c), d), e) Spatial and monthly variation in moisture sources of Pikes Peak region (PKS) precipitation in May, June, and July of 2023. a) Map of evaporative sources of PKS precipitation accumulating from May through July of 2023. b) Monthly regional contribution to the PKS in volume of water vapor ($m^3$). c) Cumulative regional evaporative contribution across May, June and July of 2023 to PKS precipitation in volume of water vapor ($m^3$). d) Monthly regional evaporative contribution as a percent of total monthly evaporative contribution. e) Cumulative regional contribution as a percent of total monthly evaporative contribution. Sink region outlined in red.

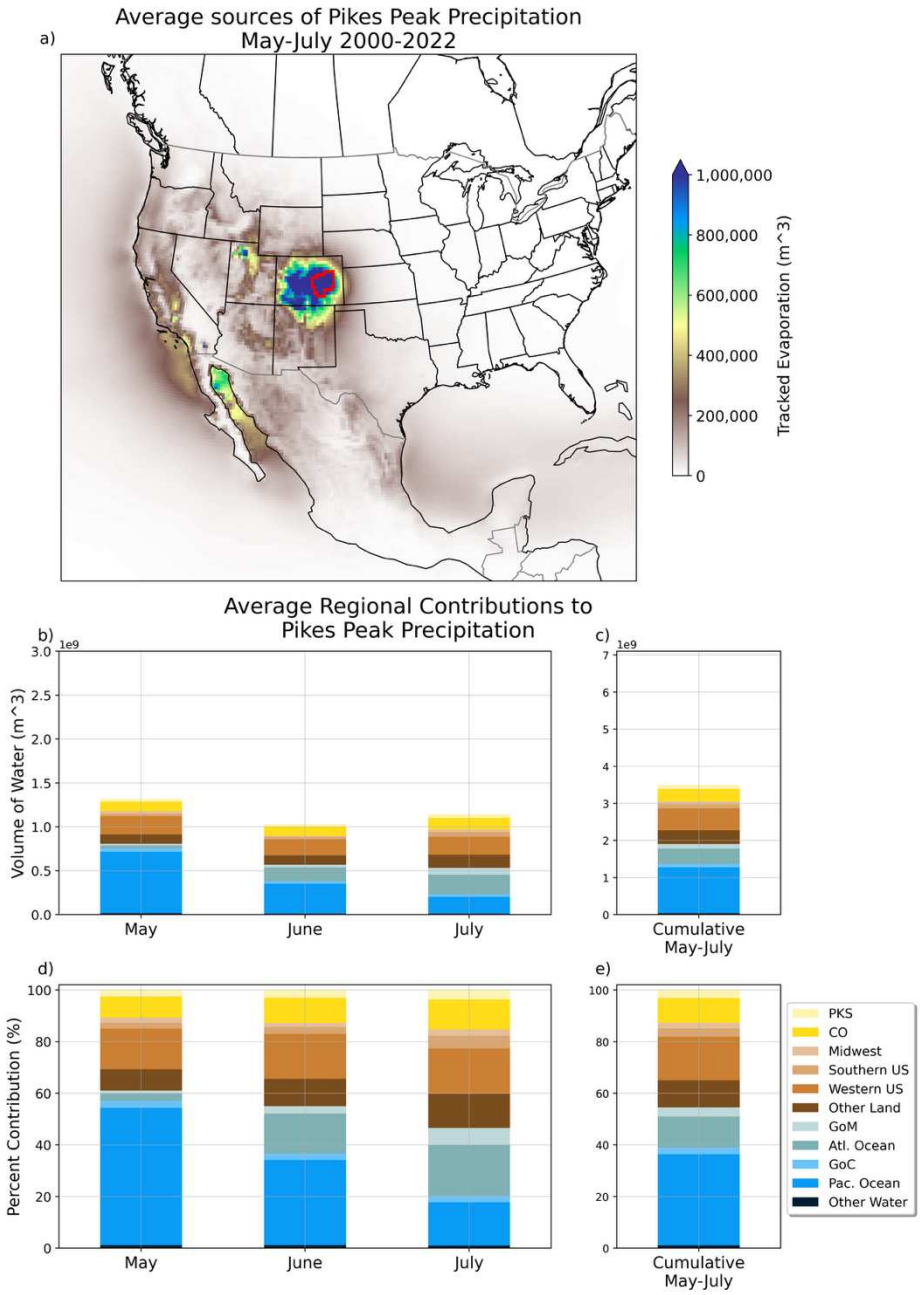


**Figure A.6.2:** (a), (b), (c) Spatial and monthly variation of Pikes Peak (PKS) moisture sources averaged from 2000-2022. (a) Map of average tracked evaporation accumulating from May through July. (b) Average monthly regional contributions to the PKS in volume of water vapor ($m^3$). (c) Average cumulative regional contribution across May, June and July to PKS precipitation in volume of water vapor ($m^3$). Sink region outlined in red.

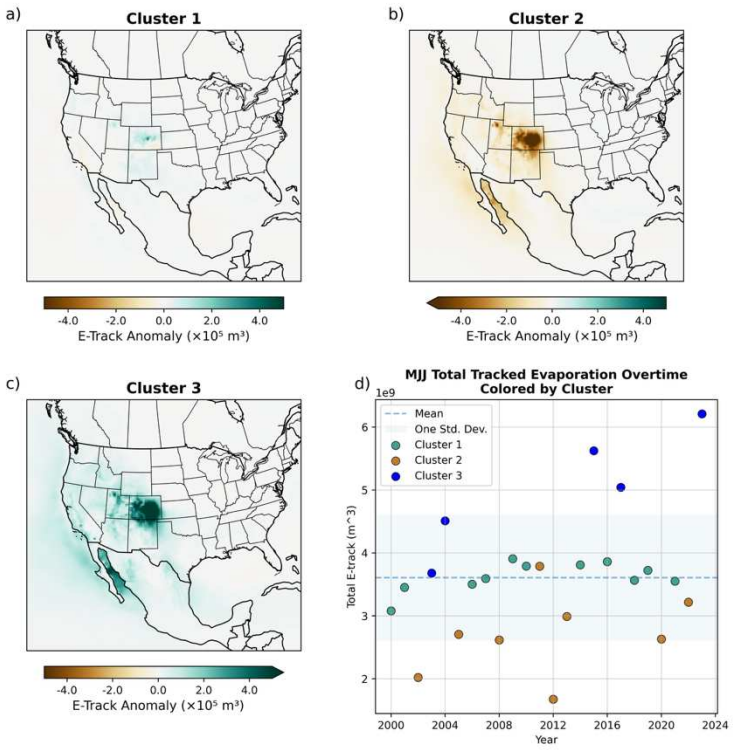


**Figure A.6.3:** Spatiotemporal patterns of MJJ evaporation anomalies of Pikes Peak (PKS) precipitation from k-means Clustering. (a), (b), (c) Cluster average MJJ moisture contribution. (d) MJJ total precipitation (spatially summed e-track) overtime colored by the assigned cluster.

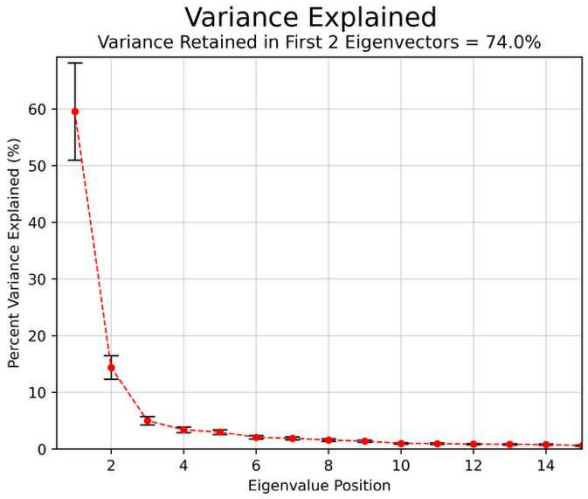


**Figure A.6.4:** Results from EOF analysis on the Pikes Peak region (PKS). Percent variance explained (PVE) by eigenvectors ranked from least to greatest eigenvalue. Error bars represent 95% confidence bounds as calculated in North et al. (1982) assuming that each MJJ season is independent of one another.

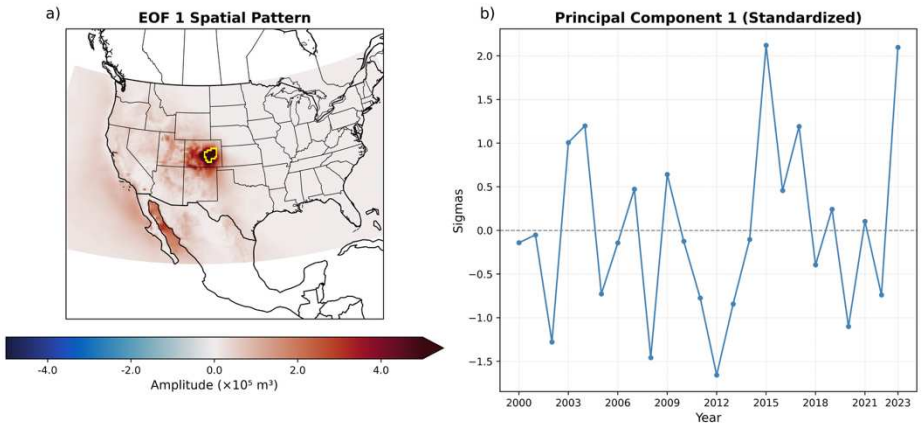


**Figure A.6.5:** (a) Spatial pattern of the first empirical orthogonal function (EOF1) of MJJ tracked evaporation anomalies for the Pikes Peak region (PKS) from 2000–2023. (b) Standardized principal component time series (PC1) corresponding to EOF1. Sink region marked in yellow.

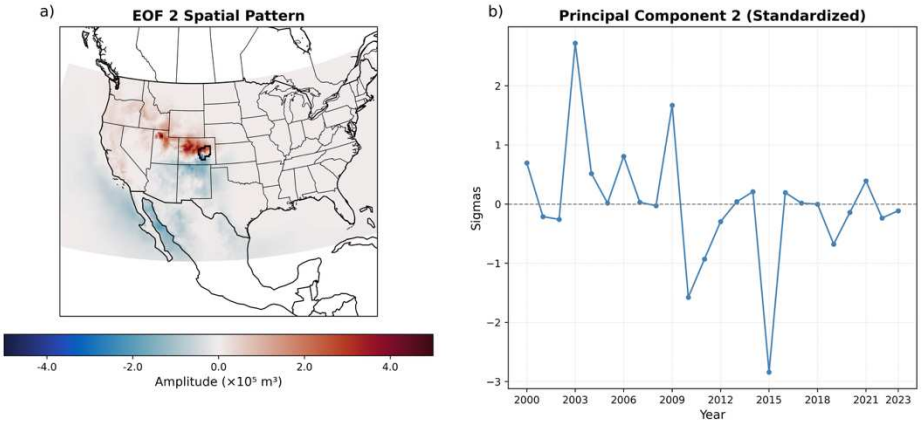


**Figure A.6.6:** (a) Spatial pattern of the first empirical orthogonal function (EOF2) of MJJ tracked evaporation anomalies for the Pikes Peak region (PKS) from 2000–2023. (b) Standardized principal component time series (PC2) corresponding to EOF2. Sink region outlined in black.